

Constraining non-unitary neutrino mixing using matter effects in atmospheric neutrinos at INO-ICAL

Sadashiv Sahoo^{a,b}, Sudipta Das^{a,b}, Anil Kumar^{a,b}
and Sanjib Kumar Agarwalla^{a,b,c}

^a*Institute of Physics, Sachivalaya Marg, Sainik School Post,
Bhubaneswar 751005, India*

^b*Homi Bhabha National Institute,
Anushakti Nagar, Mumbai 400094, India*

^c*Department of Physics & Wisconsin IceCube Particle Astrophysics Center,
University of Wisconsin, Madison, WI 53706, U.S.A*

E-mail: sadashiv.sahoo@iopb.res.in, sudipta.d@iopb.res.in,
anil.k@iopb.res.in, sanjib@iopb.res.in

ABSTRACT: The mass-induced neutrino oscillation is a well established phenomenon that is based on the unitary mixing among three light active neutrinos. Remarkable precision on neutrino mixing parameters over the last decade or so has opened up the prospects for testing the possible non-unitarity of the standard 3ν mixing matrix, which may arise in the seesaw extensions of the Standard Model due to the admixture of three light active neutrinos with heavy isosinglet neutrinos. Because of this non-unitary neutrino mixing (NUNM), the oscillation probabilities among the three active neutrinos would be altered as compared to the probabilities obtained assuming a unitary 3ν mixing matrix. In such a NUNM scenario, neutrinos can experience an additional matter effect due to the neutral current interactions with the ambient neutrons. Atmospheric neutrinos having access to a wide range of energies and baselines can experience a significant modifications in Earth's matter effect due to NUNM. In this paper, we study in detail how the NUNM parameter α_{32} affects the muon neutrino and antineutrino survival probabilities in a different way. Then, we place a comparable and complementary constraint on α_{32} in a model independent fashion using the proposed 50 kt magnetized Iron Calorimeter (ICAL) detector under the India-based Neutrino Observatory (INO) project, which can efficiently detect the atmospheric ν_μ and $\bar{\nu}_\mu$ separately in the multi-GeV energy range. Further, we discuss the advantage of charge identification capability of ICAL and the impact of uncertainties in oscillation parameters while constraining α_{32} . We also compare the α_{32} sensitivity of ICAL with that of future long-baseline experiments DUNE and T2HK in isolation and combination.

KEYWORDS: Neutrino Mixing, Non-Standard Neutrino Properties

ARXIV EPRINT: [2309.16942](https://arxiv.org/abs/2309.16942)

Contents

1	Introduction and motivation	1
2	Formalism of non-unitary neutrino mixing (NUNM)	3
3	Atmospheric neutrinos: a unique tool to probe NUNM	7
4	Simulation of neutrino events at the ICAL detector	10
5	Statistical analysis	14
6	Results	15
6.1	Effective regions in $(E_\mu^{\text{rec}}, \cos\theta_\mu^{\text{rec}})$ plane to constrain α_{32}	15
6.2	Impact of oscillation parameter marginalization in constraining α_{32}	17
6.3	Advantage of having charge identification (CID) capability	17
6.4	Constraints on α_{32} as a function of true $\sin^2\theta_{23}$	19
6.5	One-to-one comparison of ICAL with the future long-baseline setups	19
6.6	Sensitivities in $ \alpha_{32} $ and ϕ_{32} plane	22
7	Concluding remarks	24
A	A brief discussion on lower-triangular formulation of NUNM	26
B	Effective ν_μ survival probability in the presence of NUNM	29
C	Impact of new physics phase ϕ_{32} on the ν_μ survival probability	32

1 Introduction and motivation

The Standard Model (SM) of particle physics is one of the most successful models that describe the interactions of the most fundamental building blocks of our observable universe [1]. It has unambiguously established the connection between the local gauge symmetries and the three fundamental force carriers (spin-1 bosons): gluons (g) for strong, W^\pm , and Z^0 for weak and photons (γ) for electromagnetic interactions, under the $SU(3)_C \times SU(2)_L \times U(1)_Y$ representation of the gauge group, where C stands for color-charge, L corresponds to the weak isospin, and Y denotes the quantum number weak hypercharge. The fundamental principles of gauge invariance prescribe that all the terms in the Lagrangian, including the mass terms, must obey the local gauge symmetry. Since the SM does not contain right-handed neutrinos, as a consequence, neutrinos are massless in the tree-level SM Lagrangian. Even at the loop level, the SM content fails to generate neutrino

mass due to the violation of the total lepton number by two units. However, the compelling evidence of neutrino oscillations from several pioneering experiments involving solar [2–9], reactor [10–17], atmospheric [18–22], and accelerator [23–28] neutrinos indicate that they must have non-zero non-degenerate tiny masses and should mix with each other. This novel phenomenon of neutrino-flavor transition can be effectively parameterized in terms of the three mixing angles (θ_{12} , θ_{13} and θ_{23}), two independent mass-squared splittings (Δm_{21}^2 and Δm_{31}^2), and one leptonic Dirac CP phase (δ_{CP}). After a remarkable discovery of neutrino oscillation phenomena [29, 30], we are now in the precision era of neutrino physics where only a few oscillation parameters are yet to be measured precisely, such as δ_{CP} , the octant of θ_{23} , and the neutrino mass ordering, i.e., the sign of Δm_{31}^2 . Neutrinos are massless in the SM, and the exclusive lab-based evidence of the non-zero neutrino mass as required by neutrino oscillation indicates the pressing need for theories beyond the Standard Model (BSM) to accommodate non-zero neutrino mass and mixing. Therefore, neutrino oscillation can act as a unique probe to study various BSM scenarios.

The precision data on the Z-decay width at the e^+e^- collider at LEP suggest that there can be only three light active flavor neutrinos i.e., $N_{\nu_{\text{active}}} = 2.9840 \pm 0.0082$ [31]. However, there are some anomalous results from the experiments such as LSND [32, 33], MiniBooNE [34, 35], Gallium radioactive source experiments GALLEX [36], SAGE [37], and BEST [38], and Neutrino-4 [39] point towards oscillations with a significantly large mass-squared difference of $\Delta m^2 \sim 1 \text{ eV}^2$ as compared to the standard solar and atmospheric mass-squared splittings. These anomalous results observed at the short-baseline experiments suggest the existence of a fourth neutrino mass eigenstate ν_4 at the eV-scale which has to be gauge singlet because of the bounds on the number of weakly-interacting light neutrino state from the LEP experiment [31]. This gauge-singlet neutrino known as the “sterile” neutrino can reveal its existence via active-sterile mixing. Also, an unidentified emission line in the X-ray spectra of galaxy clusters is observed by the XMM-Newton and Chandra space telescopes [40, 41]. It is proposed that this X-ray emission line may originate due to the decay of a resonantly-produced keV-scale sterile neutrino dark matter [42–45]. These heavy sterile neutrinos appear naturally in various BSM scenarios which are responsible for generating small neutrino masses¹ (e.g. seesaw) [48–56] and their admixture with the three light active neutrinos may cause deviations from unitarity of the standard 3ν mixing matrix. This unitarity violation of the lepton mixing matrix can affect the oscillation probabilities of three active neutrinos [57–60].

In this paper, we study in detail the impact of NUNM in three-neutrino oscillations in a model independent fashion in the context of the proposed 50 kt iron calorimeter (ICAL) detector at the India-based Neutrino Observatory (INO) [61] using atmospheric neutrinos. Here, we show how the atmospheric neutrinos having access to a wide range of baselines and energies, can feel the presence of NUNM during their oscillations. The ICAL detector is designed to have a magnetic field of 1.5 T [62] which enables ICAL to distinguish between μ^- and μ^+ events produced from the interactions of atmospheric ν_μ

¹Several BSM possibilities can be introduced in the framework of effective field theory such as the effective lepton-number-violating dimension-five Weinberg operator which may account for the small neutrino masses [46, 47].

and $\bar{\nu}_\mu$, respectively. This charge identification (CID) capability helps ICAL to achieve its primary goal of determining the neutrino mass ordering² by observing atmospheric ν_μ and $\bar{\nu}_\mu$ separately in the multi-GeV energy range over a wide range of baselines [63]. The ICAL has excellent detector resolutions to measure momenta and directionality of μ^- and μ^+ [64]. It can also measure the energies of hadron showers that are produced during atmospheric neutrino interactions [65]. Using the ICAL detector response, the ICAL collaboration has performed a plethora of studies to measure the standard three-flavor oscillation parameters as well as to probe several BSM scenarios [63, 66–96]. Using 500 kt·yr exposure of ICAL, we study its performance in unraveling the signatures of NUNM and demonstrate the importance of its CID capability.

We start this paper with a qualitative description of the NUNM scenario and its implications on the neutrino propagation Hamiltonian in section 2. In section 3, we discuss the impact of NUNM on the survival probabilities of atmospheric ν_μ and $\bar{\nu}_\mu$. In section 4, we explain the detector configuration, simulation methodology, and events reconstruction. Section 5 deals with the statistical methodology that we use while calculating the sensitivity of ICAL towards NUNM in terms of $\Delta\chi^2$. Then, in section 6, we show the sensitivities obtained using the 500 kt·yr exposure of ICAL and discuss the impact of uncertainties of oscillation parameters, the true value of atmospheric mixing angle θ_{23} , and the advantage of using CID capability of ICAL. Further, we perform a quantitative comparison between the sensitivities towards NUNM obtained using ICAL and the next-generation long-baseline (LBL) experiments: Deep Underground Neutrino Experiment (DUNE) [97–103] and Tokai to Hyper-Kamiokande (T2HK) [104, 105]. In appendix A, we provide a brief discussion on the lower-triangular formulation of the NUNM matrix in the oscillation framework. Finally in appendix B, we derive approximate analytical expression of ν_μ survival probability in the presence of NUNM which helps us to explain the role of neutral current (NC) matter effect while probing the NUNM scenario using atmospheric neutrinos.

2 Formalism of non-unitary neutrino mixing (NUNM)

In the phenomena of mass-induced neutrino flavor oscillations, the weak flavor eigenstates, $|\nu_\beta\rangle$ where $\beta \in \{e, \mu, \tau\}$, are a linear superposition of the mass eigenstates, $|\nu_j\rangle$ where $j \in \{1, 2, 3\}$. The flavor and mass eigenstates are related to each other with the help of a 3×3 unitary mixing matrix U in the following fashion:

$$|\nu_\beta\rangle = \sum_{j=1}^3 U_{\beta j}^* |\nu_j\rangle. \quad (2.1)$$

In the above equation, the mixing matrix U is known in literature as the Pontecorvo-Maki-Nakagawa-Sakata (PMNS) matrix [106–108]. Considering the plane wave approximation of the ultra-relativistic neutrino states,³ the oscillation probability ($P_{\eta\beta}$) can be expressed

²Normal mass ordering (NMO) scenario corresponds to $m_1 < m_2 < m_3$ and inverted mass ordering (IMO) denotes the situation where $m_3 < m_1 < m_2$.

³For a detailed quantum mechanical description on mass-induced neutrino flavor transitions, see refs. [109–112].

as:

$$\begin{aligned}
P_{\eta\beta} = & \delta_{\eta\beta} - 4 \sum_{i>j}^3 \text{Re} \left[U_{\eta i}^* U_{\beta i} U_{\eta j} U_{\beta j}^* \right] \sin^2 \left(\Delta m_{ij}^2 \cdot \frac{L}{4E} \right) \\
& + 2 \sum_{i>j}^3 \text{Im} \left[U_{\eta i}^* U_{\beta i} U_{\eta j} U_{\beta j}^* \right] \sin \left(\Delta m_{ij}^2 \cdot \frac{L}{2E} \right). \tag{2.2}
\end{aligned}$$

Here, $\Delta m_{ij}^2 = m_i^2 - m_j^2$, and L and E are the propagation length and energy of neutrino, respectively. The η, β are neutrino flavor indices, i, j are neutrino mass indices, and $\delta_{\eta\beta} = \sum_j U_{\eta j} U_{\beta j}^*$. In eq. (2.2), $U \rightarrow U^*$ for antineutrinos. The second real term is CP-conserving, whereas the third imaginary term is CP-violating [113, 114]. Under the unitary neutrino mixing scenario, the total oscillation probability is conserved, i.e., $\sum_{\beta} P_{\eta\beta} = 1$. However, if NUNM is realized in Nature, the immediate consequence would be the non-conservation of the three-neutrino oscillation probabilities (see appendix A for a detailed discussion), i.e., $\sum_{\beta} P_{\eta\beta} \neq 1$. The scenario of NUNM would be obvious if the PMNS acts as a sub-matrix of a global unitary lepton mixing matrix ($\tilde{U}_{n \times n}$) that contains the admixture of a large number of neutrino species (n). Such an NUNM scenario can be naturally accounted from either the consequence of the seesaw mechanism [55, 115] or extended light neutrino mixings [57, 116]. Assuming the group of active three light neutrinos (ν_1, ν_2, ν_3) is the lightest among all possible neutrinos, and their mass-ordering uncertainties do not alter the status of the extra neutrino states. Then, the generalized linear mixing of neutrinos can be represented as:

$$\begin{aligned}
\begin{bmatrix} \nu_e \\ \nu_{\mu} \\ \nu_{\tau} \\ \vdots \end{bmatrix}_{n \times 1} &= \left(\begin{bmatrix} \tilde{U}_{e1} & \tilde{U}_{e2} & \tilde{U}_{e3} & \dots \\ \tilde{U}_{\mu 1} & \tilde{U}_{\mu 2} & \tilde{U}_{\mu 3} & \dots \\ \tilde{U}_{\tau 1} & \tilde{U}_{\tau 2} & \tilde{U}_{\tau 3} & \dots \\ \vdots & \vdots & \vdots & \ddots \end{bmatrix}_{n \times n} \xrightarrow{\text{B.R.}} \begin{bmatrix} \mathcal{N}_{3 \times 3} & \mathcal{S}_{3 \times (n-3)} \\ \mathcal{V}_{(n-3) \times 3} & \mathcal{T}_{(n-3) \times (n-3)} \end{bmatrix} \right) \cdot \begin{bmatrix} \nu_1 \\ \nu_2 \\ \nu_3 \\ \vdots \end{bmatrix}_{n \times 1}. \tag{2.3}
\end{aligned}$$

An effective block representation (B.R.) of $\tilde{U}_{n \times n}$ reveals the mode of mixings among the neutrino species. Here, \mathcal{N} represents the mixing among light neutrino states, while \mathcal{S} and \mathcal{V} are the admixture of light and heavy neutrino states, and \mathcal{T} stands for the mixing of only heavy neutrinos. For the case of three light active SM neutrinos, the mixing is given by 3×3 matrix \mathcal{N} which is the lowest order NUNM accessible in the low-energy experiments. Therefore, it make sense to replace the 3×3 unitary PMNS matrix by the new non-unitary matrix \mathcal{N} . In the literature, there are various ways to parameterize this NUNM matrix [57, 117–121]. However, Okubo’s notation [122] to decompose \mathcal{N} into a lower-triangular matrix (α) and PMNS matrix (U) is the most convenient one for the neutrino oscillation studies (see eq. (A.10) in appendix A for a detailed explanation). In this notation, \mathcal{N} can be expressed as follows [59, 115, 123–125]:

$$\mathcal{N} = (I + \alpha) \cdot U, \tag{2.4}$$

where

$$\alpha = \begin{pmatrix} \alpha_{11} & 0 & 0 \\ \alpha_{21} & \alpha_{22} & 0 \\ \alpha_{31} & \alpha_{32} & \alpha_{33} \end{pmatrix}. \quad (2.5)$$

In eq (2.4), I is the identity matrix, α is the lower-triangular matrix and U is the standard 3×3 PMNS matrix. In eq (2.5), the diagonal elements α_{ii} are real and close to zero. The off-diagonal elements α_{ij} in eq (2.5) are complex in general. A detailed discussion on the properties of α is given in the appendix of ref. [59]. In this scenario, the effective Hamiltonian of ultra-relativistic left-handed neutrinos passing through the ambient matter can be written in the three-neutrino mass basis as:

$$\mathcal{H} = \frac{1}{2E} \begin{pmatrix} 0 & 0 & 0 \\ 0 & \Delta m_{21}^2 & 0 \\ 0 & 0 & \Delta m_{31}^2 \end{pmatrix} + \mathcal{N}^\dagger \cdot \sqrt{2} G_F \begin{pmatrix} N_e - N_n/2 & 0 & 0 \\ 0 & -N_n/2 & 0 \\ 0 & 0 & -N_n/2 \end{pmatrix} \cdot \mathcal{N}, \quad (2.6)$$

where the first term represents the kinematics of the Hamiltonian in vacuum, and the last term includes the effective matter potentials for neutrinos induced due to both charged-current (CC) interactions, i.e., with ambient electrons, and neutral-current interactions, i.e., with ambient neutrons. The charged-current matter potential (V_{CC}) is quantified as $\sqrt{2}G_F N_e$, where G_F is Fermi constant and N_e is the electron number density of the matter. Unlike standard three-neutrino oscillations, the matter potential (V_{NC}) due to neutral-current interactions survives in the Hamiltonian in the case of non-unitary mixing. The strength of V_{NC} quantifies as $-G_F N_n/\sqrt{2}$, where N_n is the ambient neutron number density. For a given matter density ρ along the neutrino trajectory inside Earth, both the CC and NC effective matter potentials can be written as:

$$V_{CC} \approx 7.6 \times 10^{-14} \cdot Y_e \cdot \rho \text{ (g/cm}^3\text{) eV}, \quad (2.7)$$

$$V_{NC} \approx -3.8 \times 10^{-14} \cdot Y_n \cdot \rho \text{ (g/cm}^3\text{) eV}, \quad (2.8)$$

where Y_e and Y_n are the electron and neutron number fractions in the medium, respectively.⁴ For antineutrinos, $\mathcal{N} \rightarrow \mathcal{N}^*$, and both the matter potentials change sign. In the NUNM scenario, there is a critical imprint of neutral-current matter effect which is proportional to the density of the medium. Therefore, the atmospheric neutrinos propagating through a high-density medium inside Earth's core can experience significant modifications in the oscillation probabilities, which in turn, can be used to probe the NUNM scenario. In this paper, we show that at INO-ICAL, the efficient observation of atmospheric neutrinos traveling large distances inside Earth plays a crucial role in probing the possible presence of the NUNM parameter α_{32} which alters the ν_μ survival probabilities significantly.

Improved precision on the neutrino oscillation parameters over the past decade or so has opened up the possibility to test the unitarity of the PMNS matrix in the currently running and upcoming neutrino experiments. Along that direction, several studies have been performed to place bounds on the NUNM parameters using the available experimental

⁴ $Y_e = N_e/(N_p + N_n)$ and $Y_n = N_n/(N_p + N_n)$ where N_p is proton number density in the matter.

outcomes [126–129]. For an example, using the limits on appearance probabilities placed by the short-baseline (SBL) experiment NOMAD at CERN [130, 131], the authors in refs. [59, 126, 132] estimated the bound on the NUNM parameter $|\alpha_{32}| < 0.012$ at 95% confidence level. In ref. [128], the authors performed a global analysis of the results obtained from the SBL experiments: NOMAD and NuTeV, and LBL experiments: MINOS/MINOS+, T2K and NO ν A to place the limits on various NUNM parameters. They estimated a bound of $|\alpha_{32}| < 0.017$ at 99% confidence level.⁵ Using the present constraints on active-sterile mixing [133, 134], the authors in ref. [126] obtained a limit of $|\alpha_{32}| < 0.053$ at 95% C.L., which is valid for $\Delta m_{41}^2 \sim 0.1 - 1 \text{ eV}^2$. There, the authors also estimate a future constraint on α_{32} of around ≤ 0.3 at 90% C.L. using the LBL setup of DUNE [97–103]. Exploiting the synergies among the next-generation LBL experiments DUNE, T2HK [105, 135], and T2HK with another detector in Korea [104], the authors in ref. [123] derive a future bound of $|\alpha_{32}| < 0.27$ at 90% confidence level. Using the projected data from near and far detectors of the proposed ESS ν SB long-baseline setup, the authors in ref. [136] estimated the improved limits on various NUNM parameters. In ref. [137], the authors estimated a future bound of $|\alpha_{32}| < 0.048$ and $|\alpha_{32}| < 0.043$ at 90% confidence level, using FASER ν and FASER ν 2 detector setups, respectively. Apart from neutrino oscillation experiments, the NUNM parameters are also tightly constrained by several non-oscillation experiments. In ref. [129], the authors placed a bound of $|\alpha_{32}| < 0.011$ at 95% C.L. in the generic unitarity violation scenario, using the current flavor and electroweak precision data. This bound becomes even more stringent while considering some specific neutrino mass models. For an example, if the SM contents are extended with three heavy right-handed neutrinos in the low-scale seesaw models, then the electroweak data place a constraint on $|\alpha_{32}| < 1.2 \times 10^{-3}$ at 95% confidence level [126]. In our conclusion section, we show a comparison between all the existing and future limits on $|\alpha_{32}|$, and the expected bounds that we obtain in the present work using the proposed ICAL detector.⁶

Note that the tau neutrino row of the lepton mixing matrix is not well constrained under the assumption of NUNM. Lately, several neutrino oscillation experiments have revealed the appearance of tau neutrinos in their data sets, for an example, LBL experiment OPERA [138], atmospheric neutrino experiments Super-Kamiokande [139], IceCube-DeepCore [140], and KM3NeT/ORCA6 [141], and astrophysical tau neutrinos at IceCube [142, 143]. Undoubtedly, these new data sets involving tau neutrinos have improved our knowledge of the tau neutrino part of the lepton mixing matrix [144, 145], which in turn can shed light on the possible non-unitarity of the neutrino mixing matrix. Future neutrino experiments such as IceCube-Upgrade [146], IceCube-Gen2 [147], KM3NeT/ORCA [148], T2HK [105], DUNE [149], and INO-ICAL [93] are also expected to provide crucial insights on the tau neutrino matrix elements.

⁵Note that while analysing the neutral-current data of MINOS/MINOS+, the authors in ref. [128] used the triangular inequalities $\alpha_{ij} \leq \sqrt{1 - (1 + \alpha_{ii})^2} \sqrt{1 - (1 + \alpha_{jj})^2}$ to derive the limit on $|\alpha_{32}|$.

⁶In the present study, we do not consider the triangular inequalities while estimating the future constraints on α_{32} . We perform our analysis in a model independent fashion with one-parameter-at-a-time using the standalone INO-ICAL atmospheric neutrino setup, assuming a generic unitarity violation. Since other NUNM parameters are considered to be zero, triangular inequalities are not relevant in our analysis.

$\sin^2 2\theta_{12}$	$\sin^2 \theta_{23}$	$\sin^2 2\theta_{13}$	δ_{CP}	Δm_{21}^2 (eV ²)	Δm_{32}^2 (eV ²)	Mass Ordering
0.855	0.5	0.0875	0	7.4×10^{-5}	2.46×10^{-3}	Normal (NMO)

Table 1. The benchmark values of neutrino oscillation parameters used in this analysis, which agree with the current global fit values [150–153].

3 Atmospheric neutrinos: a unique tool to probe NUNM

The primary cosmic rays once enter into the atmosphere of Earth, interact with air nuclei in the high-altitude atmosphere producing mainly pions and less abundantly kaons [154]. These mesons for an example π^+ decays to a muon (μ^+) and a muon neutrino (ν_μ). This secondary muon is unstable and can further decay to a positron (e^+), a muon antineutrino ($\bar{\nu}_\mu$), and an electron neutrino (ν_e). Similarly, π^- also goes through the charge conjugate decay chain. Tiny contribution also comes from the kaon decay. The energy of atmospheric neutrino ranges from a few MeV to more than hundreds of TeV. They arrive at the detector from all possible directions traveling a wide range of path lengths starting from an atmospheric height of 15 km (in the downward direction) to as large as the diameter of Earth (in the upward direction). It allows us to explore the impact of various new physics scenarios including the NUNM hypothesis (main thrust of this paper) on neutrino flavor oscillations for several values of $L(\text{km})/E(\text{GeV})$ with an emphasis in the multi-GeV energy range for a detector like ICAL.

The ICAL detector is designed to efficiently detect μ^- and μ^+ events produced during the charged-current interactions of ν_μ and $\bar{\nu}_\mu$, respectively (see discussion in section 4). Around 98% of these interactions are contributed by ν_μ and $\bar{\nu}_\mu$ disappearance channels. In the expression of survival probability of muon neutrino, $P(\nu_\mu \rightarrow \nu_\mu)$, the real component of the NUNM parameter α_{32} has the prominent effect at the leading order and it couples directly with the matter effect term driven by neutral-current interactions inside Earth [123]. Therefore, in this paper, we primarily focus on the NUNM parameter α_{32} and consider it to be real having both negative and positive values. Later, we also address in detail the impact of the complex phase ϕ_{32} associated with the NUNM parameter α_{32} ($\equiv |\alpha_{32}|e^{-i\phi_{32}}$). Note that while focusing on α_{32} , all other NUNM parameters are considered to be zero. During our analysis, we observe that the above-mentioned neutral-current matter potential drives the main sensitivity towards α_{32} which is also evident from eq. (3.2).

Here, we consider three-flavor neutrino oscillations in the presence of matter with the Preliminary Reference Earth Model (PREM) [155] as the density profile of Earth. For simplicity, we assume Earth’s matter to be neutral ($N_e = N_p$) and iso-scalar ($N_p = N_n$) where $Y_e \equiv Y_n \simeq 0.5$. We use benchmark values of six oscillation parameters as given in table 1. Note that the value of Δm_{32}^2 is calculated from the effective mass-squared difference (Δm_{eff}^2)⁷ whose value is taken to be 2.49×10^{-3} eV². For NMO, we use the

⁷The effective mass-squared difference Δm_{eff}^2 is defined in terms of Δm_{32}^2 in the following way [156, 157]:

$$\Delta m_{\text{eff}}^2 = \Delta m_{32}^2 + \Delta m_{21}^2 (\sin^2 \theta_{12} + \cos \delta_{CP} \sin \theta_{13} \sin 2\theta_{12} \tan \theta_{23}). \quad (3.1)$$

positive value of Δm_{eff}^2 , whereas for IMO, Δm_{eff}^2 is taken to be negative with the same magnitude.

In figure 1, we demonstrate the impact of non-zero α_{32} , with a representative value of 0.1, on the survival probability $P(\nu_\mu \rightarrow \nu_\mu)$ of upward-going multi-GeV ν_μ and $\bar{\nu}_\mu$ in the plane of energy and zenith angle $(E_\nu, \cos \theta_\nu)$. The left column represents ν_μ survival probabilities for the values of $\alpha_{32} = 0.1, 0$ (SI: Standard Interaction), and -0.1 in the top, middle, and bottom panels, respectively. The right column shows the same for $\bar{\nu}_\mu$. Note that the benchmark values of $\alpha_{32} = \pm 0.1$ that we use in figures 1-4 and table 2 are just for an illustration purpose. We deliberately use the values of α_{32} which are almost one order of magnitude higher than the current experimental limits. We do so to have a better visualization of the possible impact of α_{32} on the oscillograms, event distributions, and while showing effective regions in $(E_\mu^{\text{rec}}, \cos \theta_\mu^{\text{rec}})$ plane to constrain α_{32} .

Due to the effect of the NUNM parameter, the characteristic changes can be noticed in the oscillation valleys, which is a dark diagonal region with the least survival probability. It would be an almost triangular strip in a three neutrino unitary-mixing scenario in vacuum [86, 88]. Here, we see a monotonic bending of these oscillation valleys in the range of $-0.85 < \cos \theta_\nu < 0$. Such a bending appears due to the term associated with V_{NC} in eq. (2.6) that offers an additional matter potential, i.e., due to neutral-current interaction along with the standard one. The monotonicity in the bending is directly related to the density profile of the Earth because in $-0.85 < \cos \theta_\nu < 0$, the Earth matter density has almost a monotonically increasing profile [155]. However, for $-1 \leq \cos \theta_\nu \leq -0.85$, neutrinos encounter the matter density at the Earth core region, which has a sharp rise in density profile. Thus, it involves a large matter interaction potential in eq. (2.6), which may introduce an extra orientation to the oscillation valleys at $-1 \leq \cos \theta_\nu \leq -0.85$. Since, for antineutrinos, both the matter potentials change their signs, the oscillation valleys bend in the opposite direction to that of neutrinos. To get an idea of how the NUNM parameter α_{32} impacts the survival probability $P(\nu_\mu \rightarrow \nu_\mu)$ and the oscillation valley, we contemplate an effective two neutrino scenario where α_{32} affects the 2-3 sector of neutrino at the leading order.

Considering the one-mass-scale-dominance approximation, i.e., $\Delta m_{21}^2 L/E \ll \Delta m_{32}^2 L/E$, and $\sin^2 \theta_{13} \simeq 0$, the survival probability $P(\nu_\mu \rightarrow \nu_\mu)$ can be expressed for a constant matter density and $\theta_{23} = 45^\circ$ as:⁸

$$P(\nu_\mu \rightarrow \nu_\mu) = \cos^2 \left[\left(\frac{\Delta m_{32}^2}{4E} + V_{NC} \cdot \alpha_{32} \right) \cdot L \right], \quad (3.2)$$

where L is the path traversed through matter by neutrino of energy E . Using the condition of first oscillation minima in eq. (3.2), we can explain the feature of the bending of the oscillation valley due to the NUNM parameter α_{32} . Assuming the propagation length of upward-going atmospheric neutrinos⁹ to be $L \simeq |2R \cos \theta_\nu|$, and $Y_n \simeq 0.5$ with the value of

⁸For a detailed derivation of $P(\nu_\mu \rightarrow \nu_\mu)$ in an effective two-flavor scenario with NUNM, see appendix B.

⁹The propagation length of atmospheric neutrinos traveling through the Earth can be calculated as:

$$L = \sqrt{(R+h)^2 - (R-d)^2 \sin^2 \theta_\nu} - (R-d) \cos \theta_\nu, \quad (3.3)$$

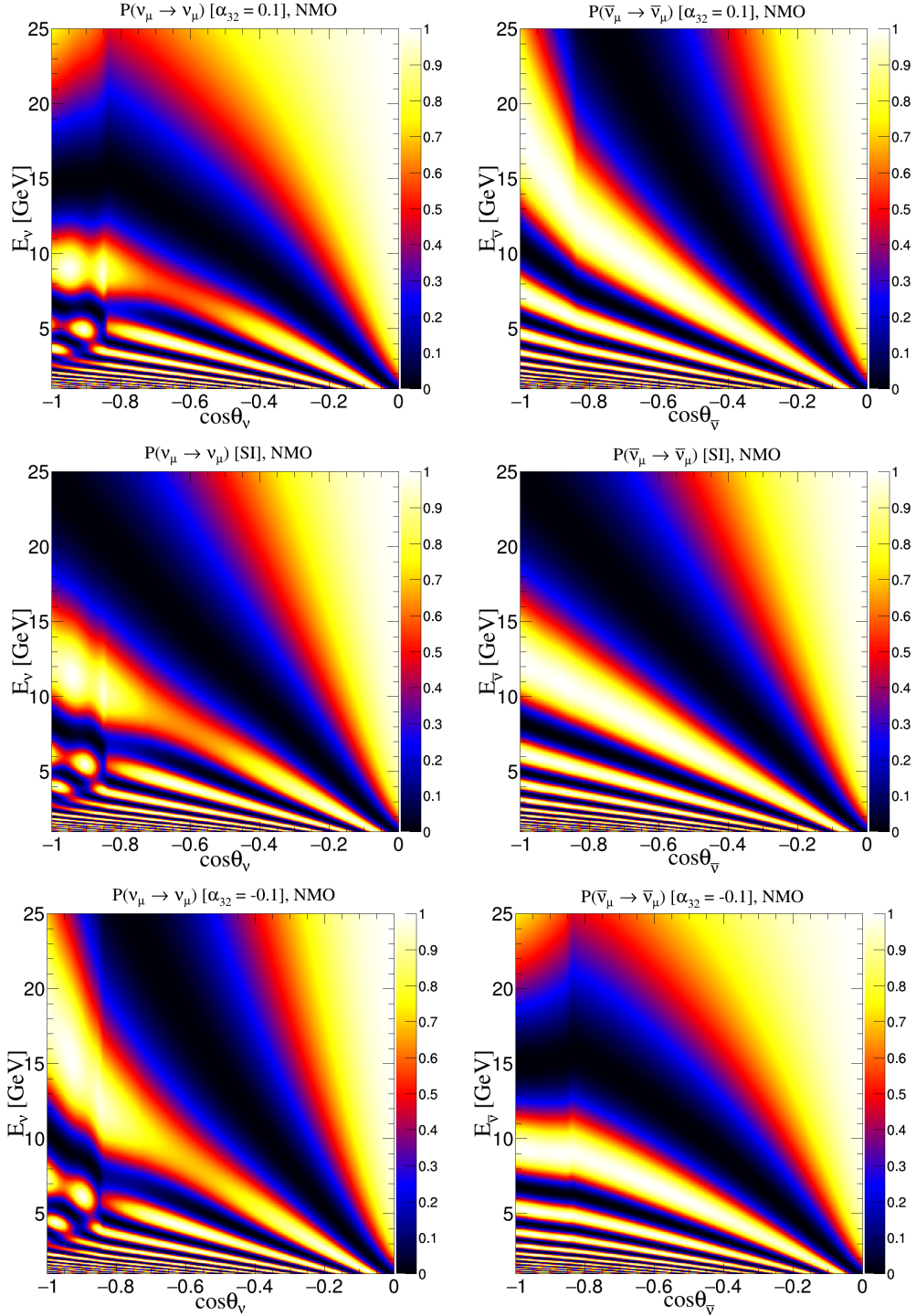


Figure 1. The survival probabilities of upward-going ν_μ (left panels) and $\bar{\nu}_\mu$ (right panels) in the $(E_\nu, \cos\theta_\nu)$ plane. We take three different values of the NUNM parameter α_{32} as 0.1, 0 (SI: Standard Interaction), and -0.1 in the top, middle, and bottom panels, respectively. We consider the Earth’s matter effect assuming the PREM profile. The values of oscillation parameters are taken from table 1.

where R is the radius of the Earth, and h and d stand for atmospheric height and detector depth from sea level, respectively. In our analysis, we consider $R = 6371$ km and $h = 15$ km while assuming that the detector (say ICAL) has been built at the sea level, i.e., $d = 0$. Using $R \gg h$ approximation, the path length of upward-going neutrinos ($\cos\theta_\nu < 0$) can be approximated to be $L \simeq |2R \cos\theta_\nu|$.

ρ using the line-averaged constant mass density approximation, the relation between $\cos \theta_\nu$ and E can be written as [88]:

$$E [\text{GeV}] \Big|_{\text{valley}} \simeq \frac{1.03 \times 10^4 \cdot \Delta m_{32}^2 [\text{eV}^2] \cdot |\cos \theta_\nu|}{1 \pm 0.78 \times \alpha_{32} \cdot \rho [\text{g/cm}^3] \cdot |\cos \theta_\nu|}. \quad (3.4)$$

Here, plus (+) sign stands for neutrino and minus (-) for antineutrino cases. For a given Δm_{32}^2 , when α_{32} has null value (for SI case), $E \propto |\cos \theta_\nu|$ which indicates the valley at first oscillation minima to be a straight line. Now, considering the values of $\alpha_{32} > 0$ for neutrinos, the denominator becomes greater than that in the SI case, which implies lower neutrino energy E and bending of oscillation valley in the downward direction. For $\alpha_{32} < 0$, the denominator decrease, and the oscillation valley bends in the upward direction. For antineutrino scenarios, the effects of non-zero α_{32} values on the $\cos \theta$ and E relation are opposite to that of neutrinos. Using eq. (3.4), we get a qualitative idea of the impacts of α_{32} on the ν_μ survival probabilities. However, to keep the analysis realistic throughout this paper, we use the three-flavor neutrino oscillation probabilities in the matter with the PREM profile.

Due to access to a wide range of baselines and energies, atmospheric neutrino detectors are blessed with a unique advantage over fixed-baseline experiments. For instance, the neutrino can travel at most ~ 1300 km through a matter density profile of $\rho^{\text{max}} < 3.0$ g/cm³ for the longest fixed-baseline experiment (DUNE) [97, 103] to be built so far. On the other hand, a plethora of atmospheric neutrinos can travel ~ 12750 km through the Earth's Core region, where they can experience a maximum matter density of ≈ 13.5 g/cm³. Such a large matter density can alter the oscillation probability significantly as compared to the long-baseline one. To showcase this fact, we plot the difference between the survival probabilities of ν_μ ($\bar{\nu}_\mu$) with NUNM and SI scenarios.

$$\Delta P = P_{\nu_\mu \rightarrow \nu_\mu} [\text{NUNM} (\alpha_{32} \neq 0)] - P_{\nu_\mu \rightarrow \nu_\mu} [\text{SI} (\alpha_{32} = 0)]. \quad (3.5)$$

In figure 2, we demonstrate the probability difference ΔP in $(E, \cos \theta)$ plane, appearing due to non-zero values of NUNM parameter α_{32} . The left (right) column shows the ΔP for upward-going ν_μ ($\bar{\nu}_\mu$) with $\alpha_{32} = 0.1$ and -0.1 in the top and bottom panels, respectively. We find the value of $|\Delta P| \lesssim 0.45$ when neutrinos and antineutrinos traverse through the Earth's mantle region, i.e., for $\cos \theta_\nu \geq -0.85$. However, this probability difference gets amplified up to 0.83 when they pass through the core of Earth, which is indeed reflected as the dark patches in the region $\cos \theta_\nu < -0.85$. Since these patterns are opposite for neutrinos and antineutrinos, the data from atmospheric neutrino detectors like ICAL, which is capable of observing ν_μ and $\bar{\nu}_\mu$ events separately, can certainly test the prospects of minimal NUNM scenario.

4 Simulation of neutrino events at the ICAL detector

To perform our analysis, we simulate neutrino events at the proposed 50 kt ICAL detector at INO [61]. ICAL would consist of three modules placed inside a cavern under the mountain in the Theni district of Tamilnadu, India. Each ICAL module of size 16 m \times 16 m \times 14.5

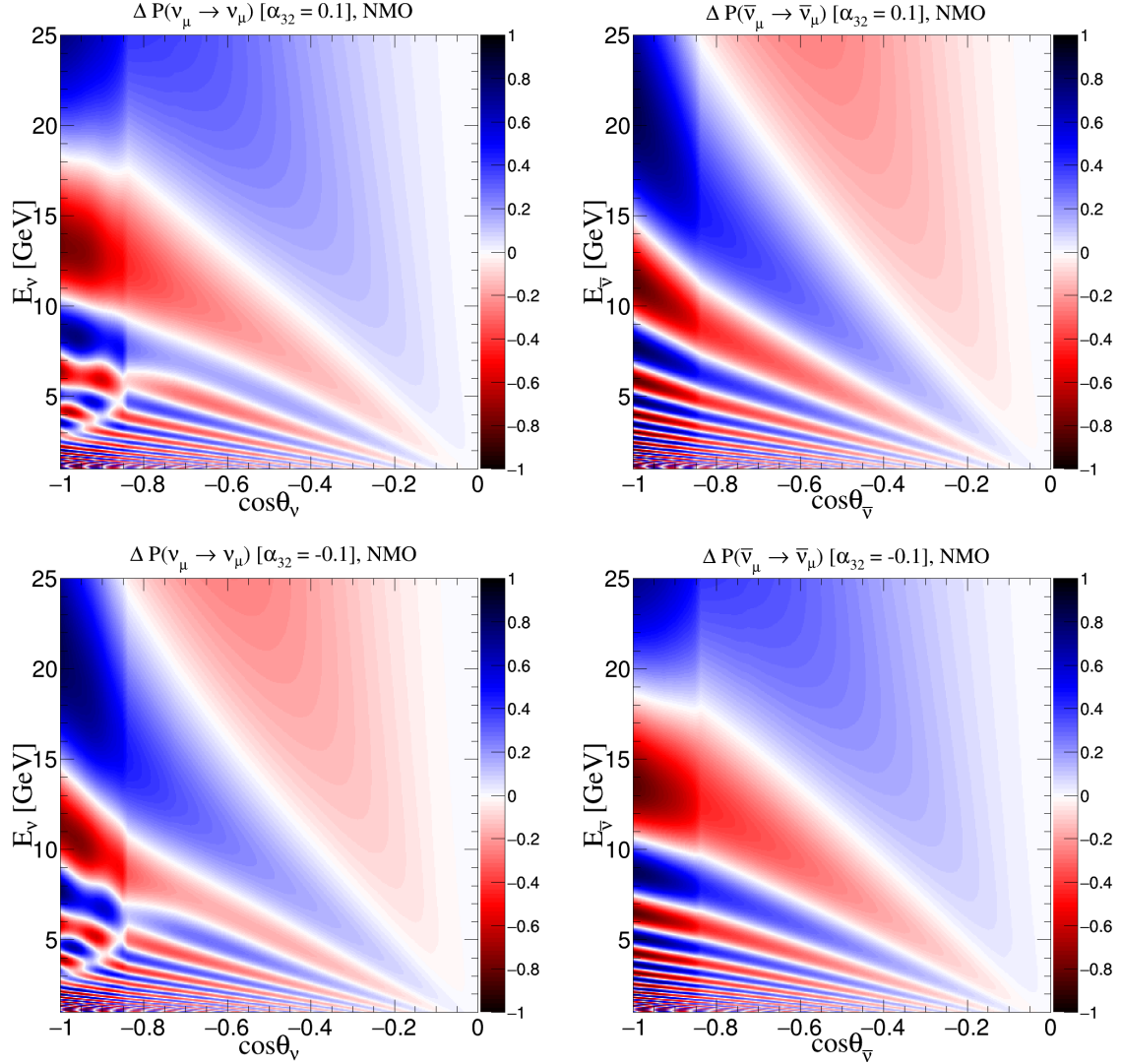


Figure 2. The survival probability difference ΔP (see (3.5)) for upward-going ν_μ (left panels) and $\bar{\nu}_\mu$ (right panels) in the $(E_\nu, \cos\theta_\nu)$ plane. We take two different values of the NUNM parameter α_{32} as 0.1 and -0.1 in the top and bottom panels, respectively. We consider the Earth’s matter effect assuming the PREM profile. The values of oscillation parameters are taken from table 1.

m contains 151 layers of magnetized iron plates of thickness 5.6 cm stacked vertically with a gap of 4 cm. These iron plates act as primary targets for the interactions of atmospheric ν_μ and $\bar{\nu}_\mu$. The resistive plate chambers (RPCs) [158] of size 2 m \times 2 m serve as active detectors and are sandwiched between two consecutive iron plates. The excellent timing resolution of RPC of ~ 1 ns [159–161], helps in the discrimination of upward-going and downward-going moun events. In these RPCs, orthogonally installed pickup strips provide the coordinates of the event hits in the $X - Y$ plane, while the layer numbers of RPCs give the Z coordinates.

ICAL can efficiently detect μ^- (μ^+) events that have been produced during the charged-current interaction of multi-GeV ν_μ ($\bar{\nu}_\mu$) via resonance and deep-inelastic scatterings. Since

Event type	Oscillation channels	$\alpha_{32} = 0$ [SI]	$\alpha_{32} = -0.1$	$\alpha_{32} = 0.1$
μ^-	$\nu_\mu \rightarrow \nu_\mu$	4318	4342	4329
	$\nu_e \rightarrow \nu_\mu$	95	99	92
	$(\nu_\mu \rightarrow \nu_\mu) + (\nu_e \rightarrow \nu_\mu)$	4413	4441	4421
μ^+	$\bar{\nu}_\mu \rightarrow \bar{\nu}_\mu$	2002	2003	2011
	$\bar{\nu}_e \rightarrow \bar{\nu}_\mu$	12	11	12
	$(\bar{\nu}_\mu \rightarrow \bar{\nu}_\mu) + (\bar{\nu}_e \rightarrow \bar{\nu}_\mu)$	2014	2014	2023

Table 2. The expected number of reconstructed μ^- (μ^+) events obtained from 500 kt-yr exposure of ICAL via both survival and appearance channels of atmospheric ν_μ ($\bar{\nu}_\mu$). We show total μ^- (top part) and μ^+ (bottom part) event rates considering $\alpha_{32} = 0$ [SI: Standard Interaction] (third column), -0.1 (fourth column), and 0.1 (fifth column). We use the values of oscillation parameters as given in table 1.

muon is the minimum ionizing particle in the multi-GeV range of energies, it leaves hits in the RPCs in the form of a long track. ICAL can measure the reconstructed muon energy in the range of 1 to 25 GeV with a resolution of about 10 to 15% [64]. The excellent resolution of the reconstructed muon zenith angle of $< 1^\circ$ helps to infer the path length traversed by the parent neutrinos [64]. The deep-inelastic scatterings of muon neutrinos can also produce hadron showers, which carry away a fraction of incoming neutrino energy. The energy deposited in the form of hadron shower can be given as $E'_{\text{had}} \equiv E_\nu - E_\mu$, where E_ν and E_μ are the true energies of incoming neutrino and generated muon, respectively.

Along with the energy and direction of the reconstructed muon, ICAL can measure the energy of the hadron shower with a resolution of about 35 to 70% [65] on an event-by-event basis. The applied magnetic field of ~ 1.5 Tesla in ICAL gives a unique feature of the charge identification (CID) capability to observe μ^- and μ^+ events separately [62]. For muons of energy of a few GeV to 50 GeV, the CID efficiency of ICAL lies between 98 to 99%, which helps in distinguishing the interactions of atmospheric ν_μ and $\bar{\nu}_\mu$ events efficiently.

In this work, we simulate the unoscillated neutrino events generated via the charged-current interactions using the NUANCE Monte Carlo neutrino event generator [162]. During this simulation, we consider the geometry of ICAL as target and use the 3D Honda flux [163, 164] of atmospheric neutrinos estimated for the proposed INO site at Theni district of Tamil Nadu, India as a source. Here, we consider the effects of solar modulation on atmospheric neutrino flux by including solar maxima for half of its exposure and solar minima for another half. A rock coverage of at least ~ 1 km from above would help in reducing the downward-going cosmic muon background at ICAL by a factor of $\sim 10^6$ [165]. The muon events entering into the detector from outside are excluded by considering only those events in the analysis that have vertices inside the detector and far from the edges. Therefore, we expect negligible background at ICAL due to the downward-going cosmic muons. We do not consider the muon events produced during the decay of tau leptons originated from ν_τ interactions because these lower energy events are expected to be small (only $\sim 2\%$ of the total up-going muon events from ν_μ interactions [166]) and mostly below the 1 GeV energy threshold of ICAL.

Since we estimate median (Asimov) sensitivities in the present work, the statistical fluctuations are needed to be suppressed. This is achieved by simulating the events for a large exposure of 50 Mt·yr which is then scaled down to 500 kt·yr for sensitivity calculations. We employ the reweighting algorithm given in refs. [67, 68] to incorporate the three-flavor neutrino oscillations for the NUNM scenario in the presence of Earth’s matter effects with PREM profile [155]. We incorporate the detector response in terms of reconstruction efficiency, CID efficiency, and resolutions of muon energy, muon zenith angle and hadron energy, using the ICAL migration matrices [64, 65] that has been approved by the ICAL Collaboration. The reconstructed μ^- and μ^+ events would have observables such as muon energy (E_μ^{rec}), zenith angle ($\cos \theta_\mu^{\text{rec}}$), and hadron energy ($E'_{\text{had}}^{\text{rec}}$).

For an exposure of 500 kt·yr, we expect about 4400 μ^- and 2000 μ^+ reconstructed events at ICAL. In table 2, we show the expected contributions to total reconstructed μ^- events via $\nu_\mu \rightarrow \nu_\mu$ survival and $\nu_e \rightarrow \nu_\mu$ appearance channels for the NUNM scenarios ($\alpha_{32} = -0.1$ and 0.1), and compare with standard scenario ($\alpha_{32} = 0$). We also show a similar comparison for the total reconstructed μ^+ events. Even though the difference in the total number of events due to the presence of non-zero α_{32} may not be large, a significant modification can be observed in the binned distribution of reconstructed events in E_μ^{rec} , $\cos \theta_\mu^{\text{rec}}$, and $E'_{\text{had}}^{\text{rec}}$.

In figure 3, we show the distributions of upward-going reconstructed μ^- (top row) and μ^+ (bottom row) events for 500 kt·yr exposure at ICAL. We consider the values of oscillation parameters mentioned in table 1 while incorporating three-flavor neutrino oscillations in the presence of matter. To plot the distributions, we use the binning scheme given in table 3. Here, we show the event distributions for three different ranges of reconstruction muon energies E_μ^{rec} which are [3, 5] GeV (left panel), [5, 11] GeV (mid panel), and [11, 25] GeV (right panel) while integrating reconstructed hadron energies ($E'_{\text{had}}^{\text{rec}}$) over 0 to 25 GeV. The black, blue, and red curves correspond to three different physics scenarios, i.e., $\alpha_{32} = 0$ (SI), 0.1, and -0.1 , respectively. The error bars represent the statistical fluctuations. The impacts of non-zero NUNM parameters ($\alpha_{32} = \pm 0.1$) can be visually appreciated when $E_\mu^{\text{rec}} > 5$ GeV, for both reconstructed μ^- and μ^+ events. Now, it is essential to note that

Observable	Range	Bin width	Total bins
E_μ^{rec} (GeV)	[1, 11]	1	10
	[11, 21]	5	2
	[21, 25]	4	1
$\cos \theta_\mu^{\text{rec}}$	[-1.0, 0.0]	0.1	10
	[0.0, 1.0]	0.2	5
$E'_{\text{had}}^{\text{rec}}$ (GeV)	[0, 2]	1	2
	[2, 4]	2	1
	[4, 25]	21	1

Table 3. The binning scheme adopted in this analysis for the three reconstructed observables E_μ^{rec} , $\cos \theta_\mu^{\text{rec}}$, and $E'_{\text{had}}^{\text{rec}}$. We use the same binning scheme for reconstructed μ^- and μ^+ events as done in ref. [89].

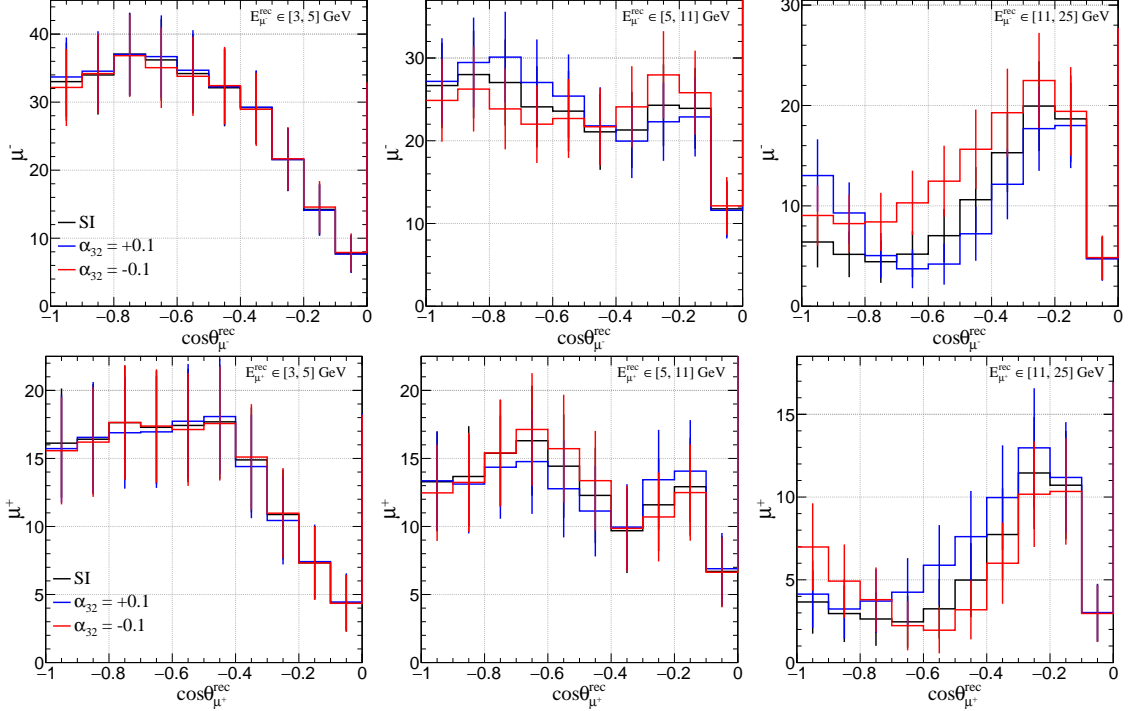


Figure 3. The upward-going reconstructed μ^- (μ^+) event distributions are shown in the top (bottom) panels for 500 kt·yr exposure of ICAL. The black, blue, and red lines in the plots correspond to SI ($\alpha_{32} = 0$), $\alpha_{32} = 0.1$, and $\alpha_{32} = -0.1$, respectively. We consider three different ranges of E_{μ}^{rec} : [3, 5] GeV (left panels), [5, 11] GeV (middle panels), and [11, 25] GeV (right panels). Note that the range of the y-axis is different in each plot. We use the values of oscillation parameters given in table 1, and the binning scheme specified in table 3, where the reconstructed hadron energy variable $E_{\text{had}}^{\text{rec}}$ is integrated over the range of 0 to 25 GeV.

for a given non-zero value of α_{32} , the event distributions of μ^- and μ^+ have opposite orientations with respect to SI. For an instance, the bin contents of blue curve ($\alpha_{32} = +0.1$) for μ^- distributions in reconstructed muon energy range [11, 25] GeV have a lower value than the SI ones, whereas these get higher for the μ^+ distributions. Such distinguishing characteristics of new physics scenarios can only be observed efficiently when the detector has the capability to identify neutrino and antineutrino events separately, like at ICAL; otherwise, it would be diluted.

5 Statistical analysis

In this analysis, we use a frequentist approach to get the median sensitivity of the detector while testing the hypothesis of non-unitary neutrino mixing. Here, we calculate the Poissonian χ^2 [167] for the reconstructed μ^- and μ^+ events by minimizing it over the systematic uncertainties. We define the χ^2 while considering three reconstructed observables: E_{μ}^{rec} , $\cos \theta_{\mu}^{\text{rec}}$ and $E_{\text{had}}^{\text{rec}}$ as follows [63]:

$$\chi^2(\mu^{\pm}) = \min_{\xi_l} \sum_{i=1}^{N_{E_{\text{had}}^{\text{rec}}}} \sum_{j=1}^{N_{E_{\mu}^{\text{rec}}}} \sum_{k=1}^{N_{\cos \theta_{\mu}^{\text{rec}}}} 2 \left[(N_{ijk}^{\text{thr}} - N_{ijk}^{\text{obs}}) + N_{ijk}^{\text{obs}} \ln \left(\frac{N_{ijk}^{\text{obs}}}{N_{ijk}^{\text{thr}}} \right) \right] + \sum_{l=1}^5 \xi_l^2, \quad (5.1)$$

where

$$N_{ijk}^{\text{thr}} = N_{ijk}^{0\text{thr}} \left(1 + \sum_{l=1}^5 \pi_{ijk}^l \xi_l \right). \quad (5.2)$$

Here, N_{ijk}^{thr} stands for the theoretically expected number of reconstructed muon events while N_{ijk}^{obs} stands for observed muon events, in a given bin of $(E_{\mu}^{\text{rec}}, \cos \theta_{\mu}^{\text{rec}}, E_{\text{had}}^{\text{rec}})$. $N_{ijk}^{0\text{thr}}$ represents the pure theoretical prediction of reconstructed events. However, the systematic uncertainties (π_{ijk}^l) can modify the pure predicted events. Thus, we adopt the pull method [168–170] to address such fluctuations. Using the pull method, we parameterize the systematic uncertainties in terms of a set of variables called pull variables ξ_l . Here, we consider a linearized approximation while accounting for the five systematic uncertainties as 20% flux normalization error, 10% error in cross section, 5% energy dependent tilt error in flux, 5% uncertainty on the zenith angle dependence of the flux, and 5% overall systematics for both ν_{μ} and $\bar{\nu}_{\mu}$ events, as prescribed in the refs. [63, 171]. The total χ^2 is a sum of $\chi^2(\mu^-)$ and $\chi^2(\mu^+)$ as:

$$\chi^2 = \chi^2(\mu^-) + \chi^2(\mu^+). \quad (5.3)$$

Now, we define the new physics sensitivity of ICAL in terms of $\Delta\chi^2$ as:

$$\Delta\chi^2 = \chi^2(\text{NUNM}) - \chi^2(\text{SI}), \quad (5.4)$$

where $\chi^2(\text{NUNM})$ and $\chi^2(\text{SI})$ are obtained by fitting the MC data with NUNM and SI scenarios, respectively. The MC data is generated assuming the SI scenario with the values of oscillation parameters as given in table 1 while considering NMO. In theory, we keep all the three diagonal NUNM parameters α_{ii} , and the two off-diagonal NUNM parameters (α_{21} , α_{31}) as zero, while considering only the non-zero real values of α_{32} . Since the statistical fluctuations are suppressed for calculating the median sensitivity of ICAL, we have $\chi^2(\text{SI}) \approx 0$. Note that the ICAL data is sensitive to $\sin^2 \theta_{23}$, Δm_{32}^2 , and the neutrino mass ordering. Therefore, in this paper, we minimize the $\Delta\chi^2$ in the fit over $\sin^2 \theta_{23}$ in the range 0.36 to 0.66, Δm_{32}^2 in the interval $[2.1, 2.6] \times 10^{-3} \text{ eV}^2$ for NMO in order to estimate the possible constraint on the NUNM parameter α_{32} . Note that we also minimize the $\Delta\chi^2$ over both the choices of mass ordering, i.e., NMO and IMO. The recipe to switch the values of Δm_{32}^2 from NMO to IMO via Δm_{eff}^2 is already discussed in section 3.

6 Results

Before we start discussing our sensitivity results on the NUNM parameter α_{32} , it is important to study the effective ranges of reconstructed muon variables $(E_{\mu}^{\text{rec}}, \cos \theta_{\mu}^{\text{rec}})$ which contribute to our sensitivity. The following subsection is devoted to shed light on this issue.

6.1 Effective regions in $(E_{\mu}^{\text{rec}}, \cos \theta_{\mu}^{\text{rec}})$ plane to constrain α_{32}

We estimate the density distributions of $\Delta\chi^2$ [$\text{GeV}^{-1} \text{ sr}^{-1}$] in the plane of $(E_{\mu}^{\text{rec}}, \cos \theta_{\mu}^{\text{rec}})$ which get contributions from each bin of separately reconstructed μ^- and μ^+ events. While estimating these density distributions of ICAL sensitivity for the NUNM scenario, we do not consider the constant contribution to $\Delta\chi^2$ from the pull penalty term mentioned in

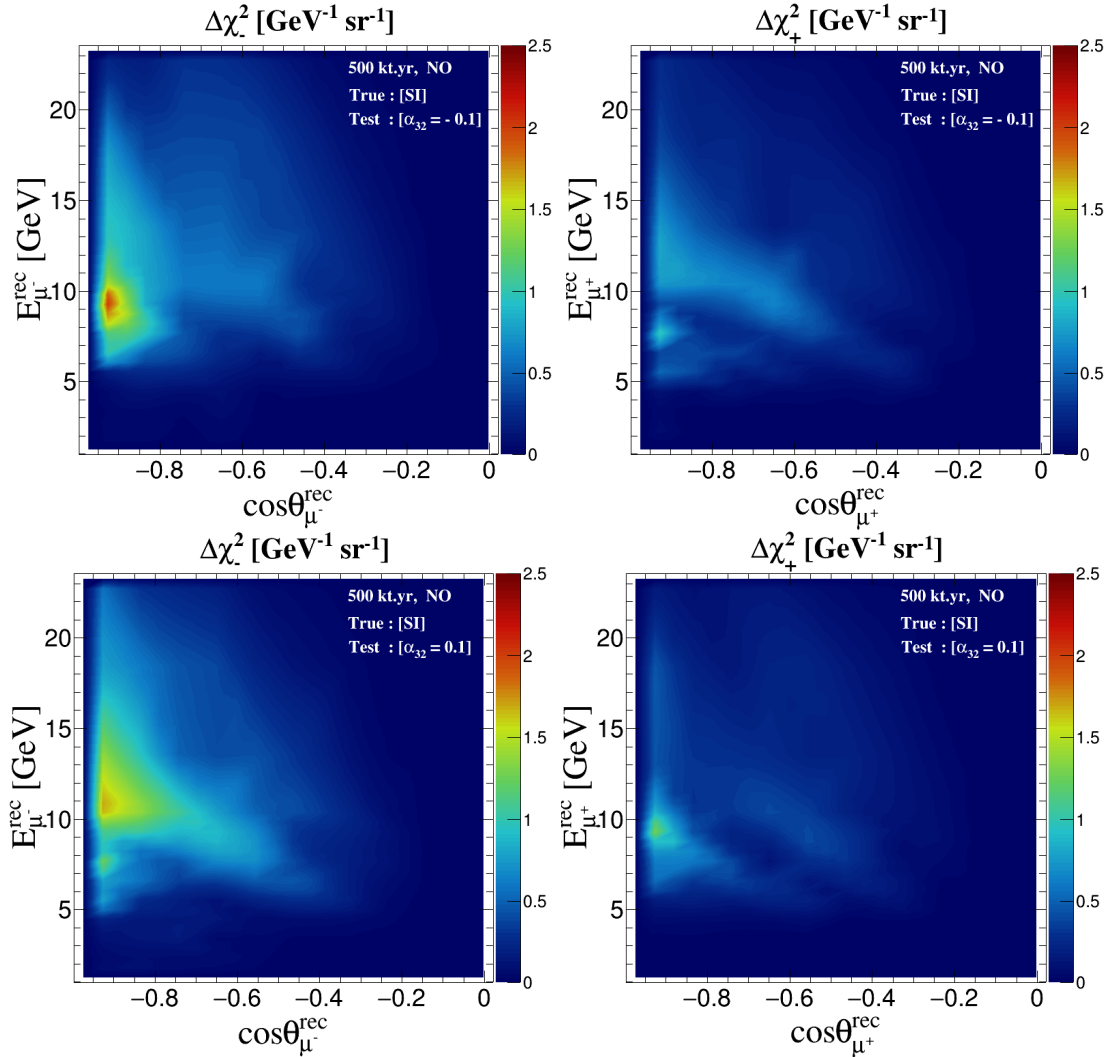


Figure 4. We show the distributions of fixed-parameter $\Delta\chi^2$ ($\Delta\chi^2_{\pm}$) in the plane of $(E_{\mu}^{\text{rec}}, \cos\theta_{\mu}^{\text{rec}})$ without the pull penalty term in the left (right) panels using 500 kt.yr exposure of the ICAL detector. Note that $\Delta\chi^2_{-}$ and $\Delta\chi^2_{+}$ are presented in the units of $\text{GeV}^{-1}\text{sr}^{-1}$ where we have divided them by $2\pi \times \text{bin area}$. The prospective data is generated assuming $\alpha_{32} = 0$, NMO (true), and using the benchmark values of oscillation parameters given in table 1. In theory, $\alpha_{32} = -0.1$ and 0.1 in the top and bottom panels, respectively.

eq. (5.1). However, we do minimize the $\Delta\chi^2$ [$\text{GeV}^{-1}\text{sr}^{-1}$] over systematic uncertainties. As far as standard oscillation parameters are concerned, we keep them fixed at values given in table 1.

In figure 4, we show the distributions of $\Delta\chi^2_{-}$ [$\text{GeV}^{-1}\text{sr}^{-1}$] and $\Delta\chi^2_{+}$ [$\text{GeV}^{-1}\text{sr}^{-1}$] in the plane of $(E_{\mu}^{\text{rec}}, \cos\theta_{\mu}^{\text{rec}})$ while considering the two values NUNM parameter ($\alpha_{32} = \pm 0.1$) for a demonstration purpose. We perform this analysis using ICAL simulated data for an exposure of 500 kt.yr. The sensitivity for μ^{-} is larger than that for μ^{+} , and this could be because of the larger statistics and significant matter effect (for NO) for the case of μ^{-} . In all the panels, ICAL sensitivity for NUNM is higher for regions of larger baselines which

correspond to the core-passing neutrinos. A significant sensitivity is obtained around the oscillation valley region, i.e., $5 \text{ GeV} \leq E_\mu^{\text{rec}} \leq 17 \text{ GeV}$ and $\cos \theta_\mu^{\text{rec}} < -0.4$.

6.2 Impact of oscillation parameter marginalization in constraining α_{32}

Over the past few decades, the precision on the three-flavor neutrino oscillation parameters have improved significantly. However, some oscillation parameters still have large uncertainties. The next-generation neutrino oscillation experiments aim to measure the value of δ_{CP} , determine the octant of θ_{23} , and resolve the issue of neutrino mass ordering. In ICAL, more than 98% of the muon events would be contributed by ν_μ survival channel and the contribution from the appearance channel is very minimal. Therefore, the ICAL sensitivities do not depend much on the value of δ_{CP} [61, 172, 173]. However, the performance of ICAL depends on the choice of $\sin^2 \theta_{23}$, Δm_{32}^2 , and the neutrino mass ordering. Therefore, in this paper, in order to estimate the possible upper bounds on the NUNM parameter α_{32} , we minimize the $\Delta\chi^2$ in the fit over $\sin^2 \theta_{23} \in [0.36, 0.66]$, $\Delta m_{32}^2 \in [2.1, 2.6] \times 10^{-3} \text{ eV}^2$, and both the choices of mass ordering. Here, the prospective MC data is generated using the benchmark values of the neutrino oscillation parameters as given in table 1 assuming NMO as true neutrino mass ordering. Note that the value of δ_{CP} is kept fixed at zero both in theory and MC data.

In figure 5, the black curve shows the constraints on the NUNM parameter α_{32} using 500 kt-yr of simulated ICAL data with the CID capability. As discussed above, while obtaining these sensitivities, the MC data is generated assuming $\alpha_{32} = 0$ (SI case) using the benchmark values of oscillation parameter given in table 1 and we minimize the $\Delta\chi^2$ over all the relevant oscillation parameters $\sin^2 \theta_{23}$, $|\Delta m_{32}^2|$, and both the choices of mass orderings in the fit. For the first time, in a model independent fashion, we evaluate the sensitivity for the NUNM parameter α_{32} as: $-0.022 \leq \alpha_{32} \leq 0.022$ at 95% C.L. with 1 d.o.f. assuming true NMO. The red curve in figure 5 is obtained in fixed-parameter scenario where we do not marginalize over relevant oscillation parameter in the fit. We observe that the red curve almost overlaps with the black curve suggesting that the marginalization over oscillation parameter does not change our sensitivity. This implies that the projected constraints on α_{32} from ICAL are quite robust against the present uncertainties in the three-flavor neutrino oscillation parameters. We also estimate the future constraints on α_{32} as $-0.025 \leq \alpha_{32} \leq 0.025$ at 95% C.L. assuming true IMO where we switch from NMO to IMO in our analysis following the prescription as described in section 3.

6.3 Advantage of having charge identification (CID) capability

The magnetic field of 1.5 T would enable ICAL to identify μ^- and μ^+ events separately by measuring the opposite directions of curvatures of their tracks. This CID capability of ICAL would help in distinguishing parent neutrinos (ν_μ) and antineutrinos ($\bar{\nu}_\mu$) which experience Earth's matter effects in a different fashion for a given mass ordering. The CID capability helps in preserving the different Earth's matter effects in neutrino and antineutrino modes separately, which in turn enhances the sensitivity of ICAL in measuring the standard three-flavor oscillation parameters and also in probing the various new-physics scenarios driven by Earth's matter effect.

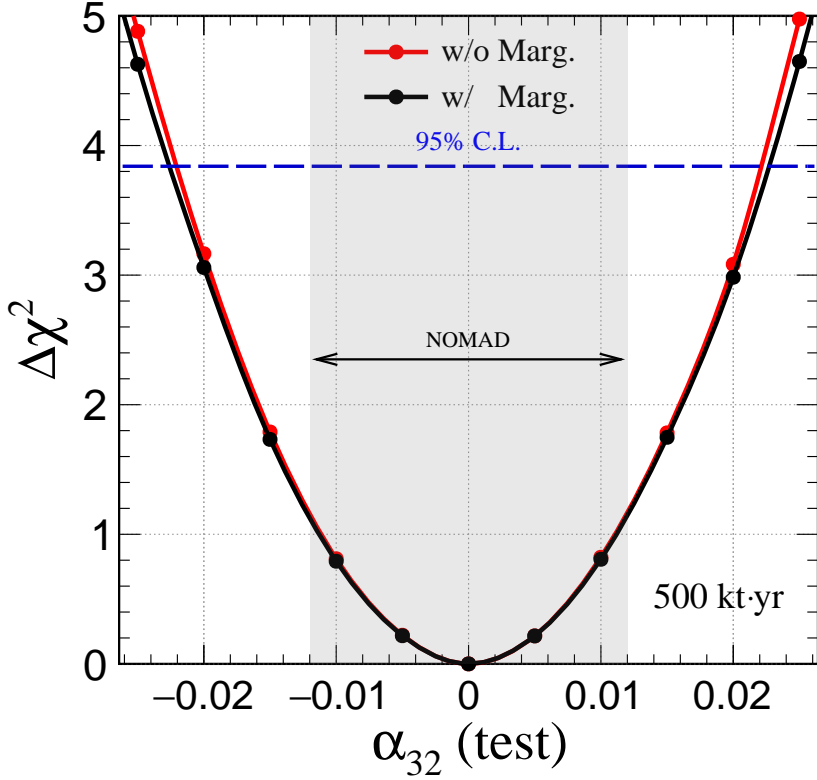


Figure 5. The possible constraints on the NUNM parameter α_{32} using 500 kt·yr of simulated ICAL data with the CID capability. The black (red) curve shows the result with (without) minimization of the $\Delta\chi^2$ over $\sin^2\theta_{23}$, $|\Delta m_{32}^2|$, and both the choices of mass orderings in the fit. The MC data is generated for the SI case ($\alpha_{32} = 0$) using the benchmark values of oscillation parameters as given in table 1. The gray band shows the present limit on α_{32} at 95% C.L. as obtained from the SBL NOMAD experiment [130, 131].

In figure 6, we show the advantage of having the CID capability of ICAL in constraining the NUNM parameter α_{32} . In this figure, we plot the $\Delta\chi^2$ (see eq. (5.4)) as a function of α_{32} in the fit where the true value α_{32} is zero in the MC data. Here, we minimize the $\Delta\chi^2$ over $\sin^2\theta_{23}$, $|\Delta m_{32}^2|$, and both the mass orderings in the fit assuming true NMO. The black curve represents the sensitivity of ICAL with the CID capability, whereas the red curve corresponds to the sensitivity without CID. We observe that in the absence of CID, the constraint on α_{32} deteriorates to $-0.056 \leq \alpha_{32} \leq 0.049$ at 95% C.L. with 500 kt·yr exposure as compared to the constraint $-0.022 \leq \alpha_{32} \leq 0.022$ that we have in the presence of CID. This happens because in the absence of CID, the reconstructed μ^- and μ^+ events get added up in each bin diluting their matter effect information which in turn deteriorates the sensitivity towards α_{32} . Also note that in the absence of CID, the α_{32} sensitivity becomes asymmetric for positive and negative values of α_{32} (test). So overall, the numbers in figure 6 indicate an improvement of around 60% in the sensitivity towards α_{32} in the presence of CID.

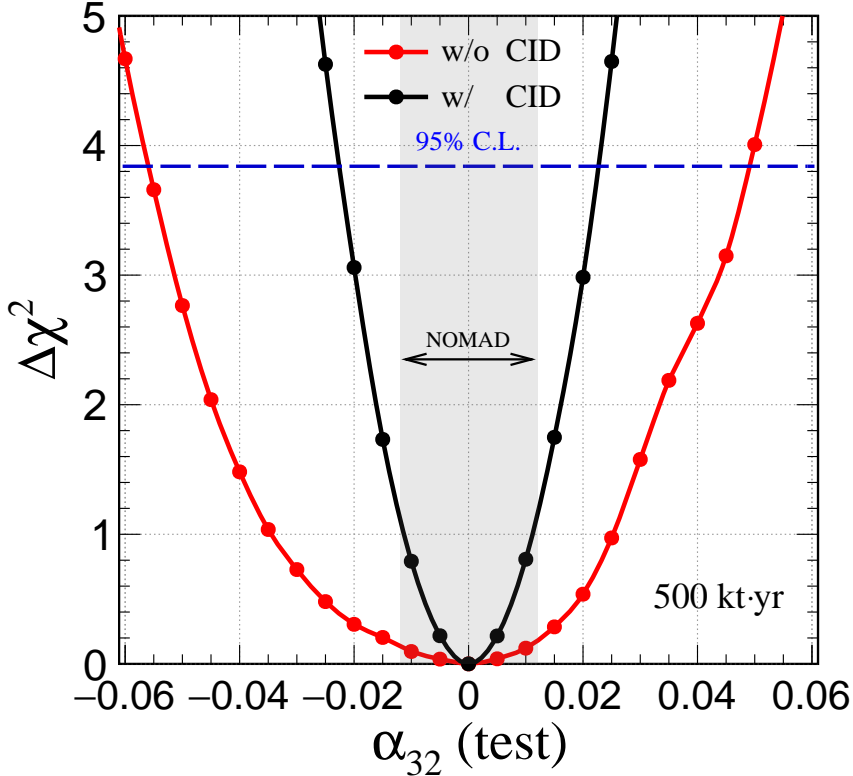


Figure 6. The possible constraints on the NUNM parameter α_{32} using 500 kt-yr of simulated ICAL data. The black (red) curve shows the result with (without) the CID capability of ICAL. In the fit, we minimize the $\Delta\chi^2$ over $\sin^2\theta_{23}$, $|\Delta m_{32}^2|$, and both the choices of mass orderings. The MC data is generated for the SI case ($\alpha_{32} = 0$) using the benchmark values of oscillation parameters as given in table 1. The gray band shows the present limit on α_{32} at 95% C.L. as obtained from the SBL NOMAD experiment [130, 131].

6.4 Constraints on α_{32} as a function of true $\sin^2\theta_{23}$

In figure 7, we examine the impact of uncertainty of the true value of θ_{23} on ICAL sensitivity to constrain α_{32} with 500 kt-yr exposure. The black curve corresponds to the sensitivity using MC data with maximal mixing, i.e., $\sin^2\theta_{23}(\text{true}) = 0.5$, whereas the red and blue curves represent that with non-maximal mixings, i.e., $\sin^2\theta_{23}(\text{true}) = 0.4$ and 0.6 , respectively. Here, we minimize $\Delta\chi^2$ over $\sin^2\theta_{23}$, $|\Delta m_{32}^2|$, and mass ordering while considering NMO as the true scenario. The ICAL sensitivity for α_{32} gets deteriorated by $\approx 14\%$ when we consider a non-maximal mixing of θ_{23} (red and blue curves) in MC data as compared to that for maximal mixing (black curve). The sensitivity for lower ($\sin^2\theta_{23} = 0.4$) and higher ($\sin^2\theta_{23} = 0.6$) octant is also similar. This happens because $P(\nu_\mu \rightarrow \nu_\mu)$ depends upon $\sin^2 2\theta_{23}$ at the leading order, enhancing the flavor transition probability, which is described in more detail in appendix B.21.

6.5 One-to-one comparison of ICAL with the future long-baseline setups

The upcoming high-precision LBL experiments DUNE [97–103] and T2HK [104, 105] are expected to provide stringent constraints on the NUNM parameters [123, 126, 174]. In

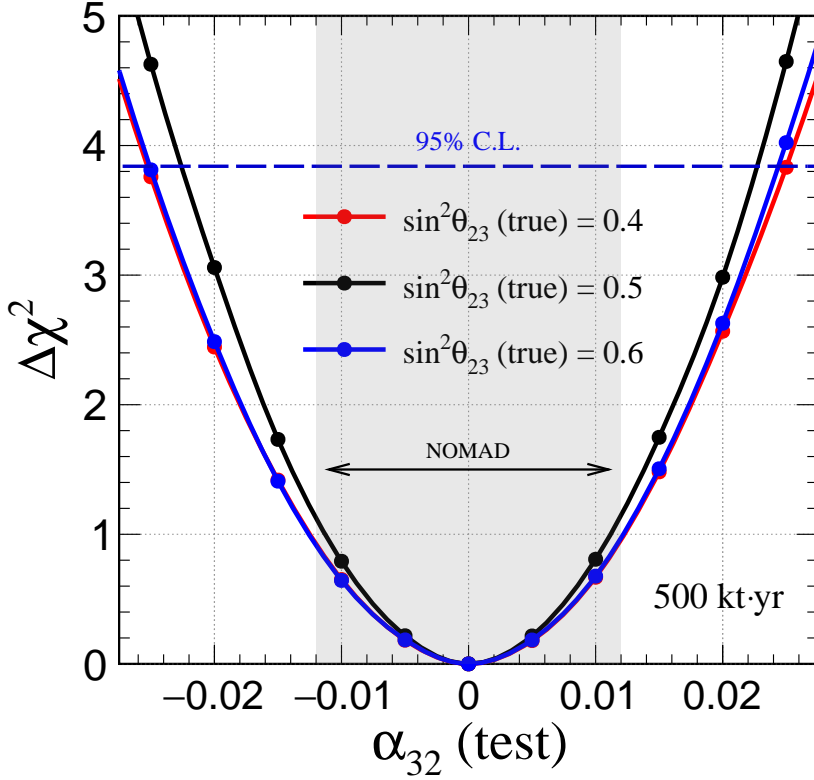


Figure 7. The possible constraints on the NUNM parameter α_{32} using 500 kt-yr of simulated ICAL data with the CID capability, while considering three different true values of $\sin^2 \theta_{23}$: 0.4 (red curve), 0.5 (black curve), and 0.6 (blue curve). In the fit, we minimize the $\Delta\chi^2$ over $\sin^2 \theta_{23}$, $|\Delta m_{32}^2|$, and both the choices of mass orderings. The MC data is generated for the SI case ($\alpha_{32} = 0$) using the benchmark values of oscillation parameters as given in table 1. The gray band shows the present limit on α_{32} at 95% C.L. as obtained from the SBL NOMAD experiment [130, 131].

this section, we provide a comparison between the future sensitivities obtained from these LBL experiments and the INO-ICAL atmospheric neutrino experiment. For this purpose, we perform a detailed simulation study to estimate the limits on the NUNM parameter α_{32} using the LBL experiments DUNE [103] and T2HK [104] in isolation and combination. To simulate the performance of DUNE having a baseline of 1300 km, we consider a total exposure of 480 kt·MW·yr which corresponds to a 1.2 MW beam of protons of 120 GeV and a 40 kt liquid-argon time-projection chamber (LArTPC) as a far detector collecting data for 10 years equally divided in neutrino (5 years) and antineutrino (5 years) modes. To simulate the prospective data of T2HK with a baseline of 295 km, we consider a total exposure of 2431 kt·MW·yr which is obtained with a 1.3 MW beam of protons of 30 GeV and a 187 kt water Cherenkov far detector collecting data for 10 years with 2.5 years of neutrino run and 7.5 years of antineutrino run. We perform the necessary simulation for these two LBL experiments using the publicly available GLoBES software [175, 176], extended with the MonteCUBES package [177]. For both these experiments, we use the benchmark values of the oscillation parameters as given in table 1 assuming true NMO

to generate the MC data with the NUNM parameter $\alpha_{32} = 0$, and consider the non-zero positive and negative real values of α_{32} in the fit. For both these LBL setups, we minimize the $\Delta\chi^2$ over $\sin^2\theta_{23}$, $|\Delta m_{32}^2|$, and both the choices of mass orderings in the fit. Similar to the ICAL analysis, we consider $\delta_{\text{CP}} = 0$ both in data and fit while obtaining the sensitivities for these LBL setups.

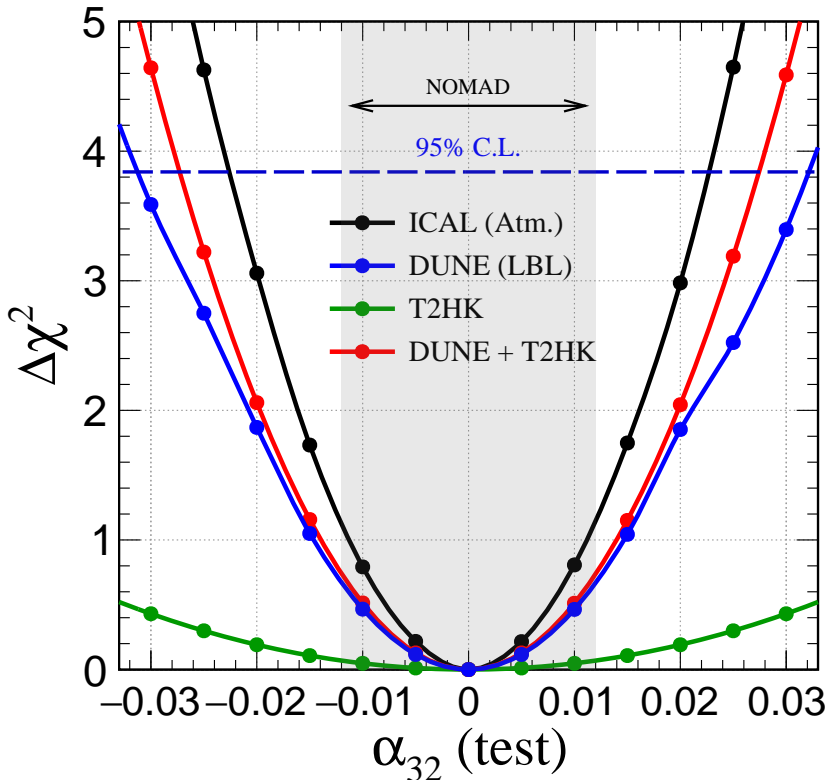


Figure 8. The possible constraints on the NUNM parameter α_{32} using 500 kt·yr of simulated atmospheric data at ICAL with the CID capability (see black curve). The blue (green) curve shows the α_{32} sensitivity of DUNE (T2HK) long-baseline setup assuming a total exposure of 480 kt·MW·yr (2431 kt·MW·yr) in 10 years. For DUNE, we assume 5 years of neutrino run and 5 years of antineutrino run. For T2HK, we consider 2.5 years of neutrino run and 7.5 years of antineutrino run. The red curve portrays the α_{32} sensitivity using the combined analysis of the long-baseline MC data from DUNE and T2HK. For all these experimental setups, we minimize the $\Delta\chi^2$ over $\sin^2\theta_{23}$, $|\Delta m_{32}^2|$, and both the choices of mass orderings. The MC data is generated for the SI case ($\alpha_{32} = 0$) using the benchmark values of oscillation parameters as given in table 1 and assuming NMO as true mass ordering. We consider $\delta_{\text{CP}} = 0$ both in data and fit while obtaining the results for all these setups. The gray band shows the present limit on α_{32} at 95% C.L. as obtained from the SBL NOMAD experiment [130, 131].

In figure 8, we show the values of minimized $\Delta\chi^2$ as a function of α_{32} (test) in fit. The black curve shows the α_{32} sensitivity of INO-ICAL atmospheric neutrino experiment considering its CID capability. The blue (green) curve reveals the α_{32} sensitivity for the standalone DUNE (T2HK) LBL setup. The red curve depicts the sensitivity for the combined analysis of DUNE and T2HK. We observe that the sensitivity from the combined DUNE + T2HK analysis is better than their individual performance. Owing to the smaller

ICAL	DUNE	T2HK	DUNE + T2HK
[-0.022, 0.022]	[-0.031, 0.032]	[-0.089, 0.089]	[-0.027, 0.027]

Table 4. A comparison between the expected constraints on the NUNM parameter α_{32} at 95% C.L. obtained from 500 kt-yr atmospheric neutrino exposure of ICAL (first column), 480 kt-MW-yr exposure of DUNE LBL setup (second column), and 2431 kt-MW-yr exposure of T2HK LBL setup (third column). The last column shows the sensitivity of α_{32} obtained from the combined analysis of DUNE and T2HK LBL data. For all the experimental setups, we minimize the $\Delta\chi^2$ over $\sin^2\theta_{23}$, $|\Delta m_{32}^2|$, and both the choices of mass orderings in the fit. The prospective MC data is generated using the benchmark values of oscillation parameters given in table 1. We consider $\delta_{\text{CP}} = 0$ both in data and fit.

baseline, and hence, less matter effect, the sensitivity of T2HK (see green curve) is significantly less as compared to DUNE (see blue curve). We also notice in this one-to-one comparison that the sensitivity of ICAL (see black curve) is slightly better than DUNE and DUNE + T2HK owing to the large matter effects via NC interactions experienced by atmospheric neutrinos at ICAL. We tabulate the constraints on the NUNM parameter α_{32} obtained from these various experiments at 95% C.L. in table 4.

So far, in this paper, we treat α_{32} as a real parameter with positive and negative values. In other words, we consider the NUNM phase ϕ_{32} associated with α_{32} (in the convention of $\alpha_{32} \equiv |\alpha_{32}|e^{-i\phi_{32}}$) to be 0 and π . Now, we study the impact of the NUNM phase ϕ_{32} on the future sensitivities towards $|\alpha_{32}|$ which can be obtained from the above-mentioned LBL and atmospheric neutrino experiments. To see the impact of the NUNM phase ϕ_{32} on the INO-ICAL analysis, we repeat our simulations for INO-ICAL by performing the minimization of the $\Delta\chi^2$ over all possible values of $\phi_{32} \in [-\pi, \pi]$ in the fit while keeping all the standard three-flavor neutrino oscillation parameters fixed in the fit for computational ease. We obtain a new constraint of $|\alpha_{32}| \leq 0.12$ at 95% C.L. using 500 kt-yr exposure of INO-ICAL. We also repeat the simulations for DUNE and T2HK in isolation and combination by performing the minimization of the $\Delta\chi^2$ over ϕ_{32} in the fit while keeping the standard three-flavor neutrino oscillation parameters fixed in the fit. While studying the impact of ϕ_{32} on the LBL setups, we also consider $\delta_{\text{CP}} = 0$ both in data and fit as we assume for ICAL. In table 5, we compare the sensitivities for $|\alpha_{32}|$ obtained from DUNE, T2HK, and DUNE + T2HK with that from ICAL by performing the minimization over ϕ_{32} in the fit. We observe that owing to Earth’s matter effects, INO-ICAL has slightly better sensitivity for $|\alpha_{32}|$ as compared to DUNE, T2HK, and their combination even after the marginalization over the phase ϕ_{32} .

6.6 Sensitivities in $|\alpha_{32}|$ and ϕ_{32} plane

In table 5, we show that how the sensitivity of standalone ICAL for constraining $|\alpha_{32}|$ gets impacted by minimizing the $\Delta\chi^2$ over the NUNM phase $\phi_{32} \in [-\pi, \pi]$. In figure 9, we show the sensitivities of ICAL in the $|\alpha_{32}|$ and ϕ_{32} plane. The solid black curves indicate that the sensitivity for $|\alpha_{32}|$ gets significantly deteriorated for $\phi_{32} \simeq \pm\pi/2$ in the fit. This can be explained from the approximate expression of the $\nu_\mu \rightarrow \nu_\mu$ survival probability derived in appendix C, where we observe that the leading term containing $|\alpha_{32}|$ has dependence of

ICAL	DUNE	T2HK	DUNE + T2HK
< 0.12	< 0.21	< 1.08	< 0.20

Table 5. A comparison between the expected constraints on $|\alpha_{32}|$ at 95% C.L. obtained after marginalizing over the NUNM phase $\phi_{32} \in [-\pi, \pi]$ using 500 kt-yr exposure of INO-ICAL atmospheric neutrino experiment (first column), 480 kt-MW-yr exposure of DUNE LBL setup (second column), and 2431 kt-MW-yr exposure of T2HK LBL setup (third column). The last column shows the sensitivity for $|\alpha_{32}|$ obtained from the combined analysis of DUNE and T2HK. For all the experimental setups, we keep the value of the oscillation parameters fixed both in data and fit at their benchmark values as given in table 1. We also consider $\delta_{\text{CP}} = 0$ both in data and fit.

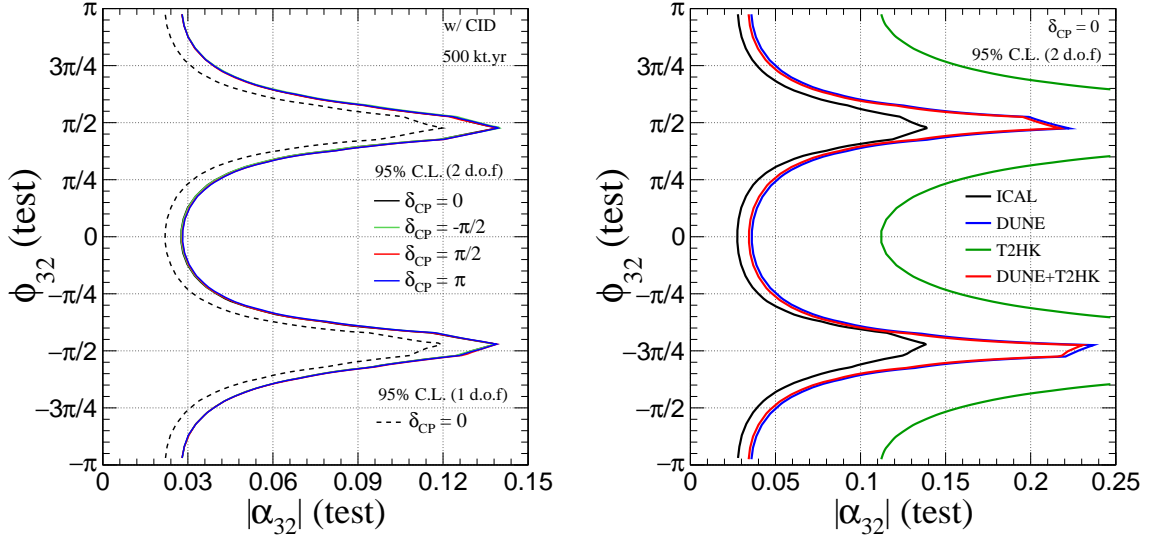


Figure 9. The left panel shows the expected constraints on the NUNM parameter α_{32} on the plane of $(|\alpha_{32}|, \phi_{32})$ using 500 kt-yr exposure of the simulated ICAL data with the CID capability. We consider four different true values of δ_{CP} : 0 (black curve), $-\pi/2$ (green curve), $\pi/2$ (red curve) and π (blue curve) at 95% C.L. (2 d.o.f), while keeping δ_{CP} fixed in the fit at its respective true values. In the fit, we also keep all other oscillation parameters fixed at their true values. Additionally, the black dashed curve shows the limits on $|\alpha_{32}|$ for 1 d.o.f. at 95% confidence level. The right panel shows the expected sensitivities for future long baseline experiments in the plane of $|\alpha_{32}|$ and ϕ_{32} . The blue (green) curve shows the sensitivity for DUNE (T2HK) long-baseline setup assuming a total exposure of 480 kt-MW-yr (2431 kt-MW-yr) in 10 years. For DUNE, we assume 5 years of neutrino run and 5 years of antineutrino run. For T2HK, we consider 2.5 years of neutrino run and 7.5 years of antineutrino run. The red curve portrays the sensitivity using the combined analysis from DUNE and T2HK. We consider $\delta_{\text{CP}} = 0$ both in MC data and fit for all these experimental setups. For both the panels, the MC data is generated for the SI scenario ($|\alpha_{32}| = 0$, $\phi_{32} = 0$) using the benchmark values of oscillation parameters as given in table 1 and assuming NMO as true mass ordering.

$\cos \phi_{32}$. Therefore, for $\phi_{32} \simeq \pm \pi/2$, the contribution from $|\alpha_{32}|$ in the survival probability almost vanishes, reducing its sensitivity near those values.

In the left panel, we show the sensitivity curves for four different true values of δ_{CP} , namely, 0 (black curve), $-\pi/2$ (green curve), $\pi/2$ (red curve) and π (blue curve) at 95%

C.L. (2 d.o.f), while δ_{CP} in fit is also kept fixed at its respective true value. We observe that our result is robust under all possible values of δ_{CP} . Therefore, in future, if the δ_{CP} found to be non-zero with a precise value, it would not impact the constraint placed by ICAL. This happens because survival channel of muon neutrino $P(\nu_\mu \rightarrow \nu_\mu)$ and $P(\bar{\nu}_\mu \rightarrow \bar{\nu}_\mu)$ contributes about 98% of the reconstructed μ^- , and μ^+ events at the ICAL detector, respectively. In the approximate expression of $\nu_\mu \rightarrow \nu_\mu$ survival probability, as shown in ref. [178], δ_{CP} appears in terms of $\cos \delta_{\text{CP}}$ which is suppressed by a factor of $\frac{\Delta m_{21}^2}{\Delta m_{31}^2} \sin \theta_{13} \simeq 0.005$. Therefore, the effect of δ_{CP} is negligible irrespective of any new physics scenario. Note that we perform this analysis in a fixed oscillation parameters scenario, as we find in figure 5 that there is no significant impact of minimization of $\Delta\chi^2$ over $\sin^2 \theta_{23}$, $|\Delta m_{32}^2|$ and both choices of mass orderings in the fit. We also show the sensitivity for 1 d.o.f at 95% C.L. as indicated by the black dashed curve, in order to have a comparison with $|\alpha_{32}|$ sensitivity shown in table 5 for 1D analysis discussed in the previous section.

In the right panel, we compare the sensitivity of ICAL with that of the next-generation long-baseline experiments DUNE, T2HK, and their combination in the $|\alpha_{32}|$ and ϕ_{32} plane at 95% C.L. (2 d.o.f.). Here, we consider the true value of $\delta_{\text{CP}} = 0$ for all the experimental setups. Similar to the observation made in section 6.5, we found that the ICAL sensitivity (shown by the black curve) is slightly better than DUNE and T2HK setups, individually and in combination.

7 Concluding remarks

The experimental evidence of the mass-induced neutrino flavor transitions places a dent on the Standard Model (SM) of particle physics and this basically opens up a gateway to the phenomenology of beyond the SM (BSM). The mixing among three light active neutrinos is described by unitary matrix. Since over the past few decades, the precision of neutrino oscillation parameters have improved significantly, it is natural to attempt to test the unitarity of mixing matrix. In this article, we study the non-unitary neutrino mixing (NUNM) scenario using atmospheric neutrinos over a wide range of baselines in a multi-GeV range of energies at the upcoming INO-ICAL detector. Here, our cornerstone is exploring the non-unitary neutrino mixing parameter α_{32} through mass-induced neutrino oscillations. We consider only the real values of α_{32} and show that ICAL can place a stringent limit on it. Here, we study the possibility of non-unitary neutrino mixing among the three SM neutrinos. We discuss in detail how the NUNM scenario can uphold the potential arising due to neutral-current interactions and can make a significant alteration in the neutrino oscillation probabilities. We explore the impact of the NUNM parameter α_{32} on the $\nu_\mu \rightarrow \nu_\mu$ survival channel and derive an approximate analytical expression for an effective two-neutrino mixing in 2-3 sector (see appendix B). We demonstrate such an effect using oscillogram of ν_μ survival probability.

We simulate the effect of the NUNM parameter α_{32} on the distribution of reconstructed muon events for the upcoming 50 kt ICAL with an exposure of 10 years. Here, we perform

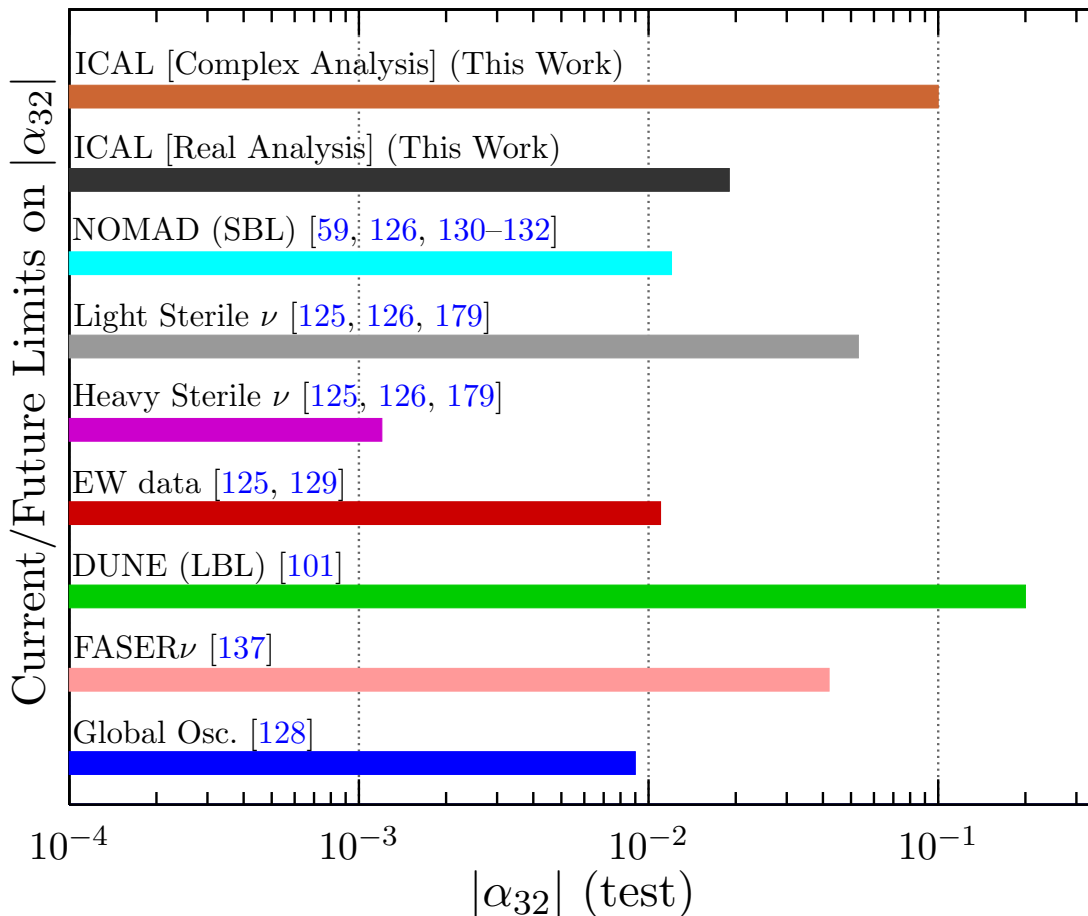


Figure 10. Comparison of the ICAL sensitivity with the well-known current and expected bounds on NUNM parameter α_{32} . Note that the mentioned bounds are at 90% C.L., except the NOMAD (SBL) and electroweak (EW) data which are calculated at 95% confidence level.

a $\Delta\chi^2$ analysis to estimate the new physics sensitivity of the INO-ICAL detector. In this work, we evaluate the sensitivity to place a limit on the NUNM parameter α_{32} using an atmospheric neutrino experiment like ICAL. We discuss the advantages of using the charge-identification feature at ICAL both at the event level and $\Delta\chi^2$ analysis. We find that the α_{32} sensitivity is robust against the minimization of $\Delta\chi^2$ over the uncertainties of atmospheric oscillation parameters. We further explore the impact of octant uncertainty of θ_{23} (true) while constraining the NUNM parameter α_{32} . Since there is literature that discusses the NUNM scenario for the mass-induced neutrino oscillations using the long-baseline experimental data and the proposed long-baseline simulated data, we perform a one-to-one comparison of the sensitivities of the future long-baseline experiments such as DUNE, T2HK as well as their combination (DUNE + T2HK) with that of ICAL. In figure 10, we show a comparison of the expected bounds on $|\alpha_{32}|$ using ICAL with its CID capability and the limits from the current and future experiments. Figure 10 reveals that if the NUNM parameter α_{32} is assumed to be real, then the proposed ICAL detector

would be able to provide a comparable and complementary constraint using atmospheric neutrinos as compared to the current limits obtained from the SBL NOMAD experiment and electroweak precision data. We also observe that the complex phase ϕ_{32} associated with α_{32} affects the ICAL sensitivity and makes the limit weaker by almost an order of magnitude.

For probing the BSM physics scenarios, it is essential to make precise measurements of oscillation parameters, and such a process will be enhanced with the detection of ν_τ events. We believe that the next-generation neutrino detectors will be capable of observing the charged-current tau events via the tau neutrino appearance channel. Such an event analysis will undoubtedly enhance the robustness of three-neutrino unitary mixing. In fact, a thorough analysis of currently acquired high-precision atmospheric neutrino data at Super-K, IceCube, DeepCore, and ORCA can definitely shed a light on the test for unitary neutrino mixing.

Acknowledgements

We thank the members of the INO-ICAL collaboration, and the anonymous referee for their valuable comments and constructive inputs. We sincerely thank A. Dighe, S. Goswami, S. Choubey, and P. Swain, A. Giarnetti for their useful comments and suggestions. We acknowledge the support of the Department of Atomic Energy (DAE), Govt. of India, under Project Identification No. RTI4002. S.K.A. gets supported by the DST/INSPIRE Research Grant [IFA-PH-12] from the Department of Science and Technology (DST), Govt. of India, and the Young Scientist Project [INSA/SP/YSP/144/2017/1578] from the Indian National Science Academy (INSA). S.K.A. acknowledges the financial support from the Swarnajayanti Fellowship Research Grant (No. DST/SJF/PSA-05/2019-20) provided by the Department of Science and Technology (DST), Govt. of India, and the Research Grant (File no. SB/SJF/2020-21/21) provided by the Science and Engineering Research Board (SERB) under the Swarnajayanti Fellowship by the DST, Govt. of India. S. Sahoo thanks the organizers of the XXV DAE-BRNS symposium 2022, IISER, Mohali, India, from 12th to 16th December 2023, for providing him an opportunity to give a talk to present the preliminary results from this work. We acknowledge the Sim01: High-Performance Computing facilities at Tata Institute of Fundamental Research, Mumbai for performing the numerical simulations.

A A brief discussion on lower-triangular formulation of NUNM

Let's consider a scenario where ' n ' numbers of neutrinos are mixing with each other via a global mixing matrix \tilde{U} that is an $n \times n$ square matrix. Recalling eq. (2.3) to represent the mixing matrix as follows:

$$\tilde{U}^{n \times n} = \begin{pmatrix} N & S \\ V & T \end{pmatrix} \equiv \left(\begin{array}{c|c} N^{3 \times 3} & S^{3 \times (n-3)} \\ \hline V^{(n-3) \times 3} & T^{(n-3) \times (n-3)} \end{array} \right). \quad (\text{A.1})$$

Here, N , S , V and T are the elements of $\tilde{U}^{n \times n}$ matrix in the form of block matrices. Now, transforming neutrino mass basis to flavor basis,

$$\begin{bmatrix} \nu_e \\ \nu_\mu \\ \nu_\tau \\ \cdot \\ \cdot \\ \cdot \\ \cdot \end{bmatrix}_{n \times 1} = \begin{bmatrix} \tilde{U}_{e1} & \tilde{U}_{e2} & \tilde{U}_{e3} & \dots & \dots & \dots \\ \tilde{U}_{\mu1} & \tilde{U}_{\mu2} & \tilde{U}_{\mu3} & \dots & \dots & \dots \\ \tilde{U}_{\tau1} & \tilde{U}_{\tau2} & \tilde{U}_{\tau3} & \dots & \dots & \dots \\ \dots & \dots & \dots & \dots & \dots & \dots \\ \dots & \dots & \dots & \dots & \dots & \dots \\ \dots & \dots & \dots & \dots & \dots & \dots \\ \dots & \dots & \dots & \dots & \dots & \dots \end{bmatrix}_{n \times n} \cdot \begin{bmatrix} \nu_1 \\ \nu_2 \\ \nu_3 \\ \cdot \\ \cdot \\ \cdot \\ \cdot \end{bmatrix}_{n \times 1} \quad (\text{A.2})$$

In this representation, there are blocks showing the current accessibility regime, i.e., we can detect ν_e , ν_μ , and ν_τ via inverse-beta decay processes, and we have precisely measured the magnitudes of solar and atmospheric mass-squared splittings (Δm_{21}^2 and Δm_{31}^2) which are related to ν_1 , ν_2 and ν_3 neutrino mass states. In the accessible neutrino energy, the Hamiltonian in mass-basis can be represented in a block matrix as follows:

$$H_{n \times n}^m = \frac{1}{2E} \cdot \begin{bmatrix} \delta m^2 & 0 \\ 0 & \Delta M^2 \end{bmatrix}_{n \times n} \quad \text{where } \delta m^2 = \begin{bmatrix} 0 & 0 & 0 \\ 0 & \Delta m_{21}^2 & 0 \\ 0 & 0 & \Delta m_{31}^2 \end{bmatrix}_{3 \times 3},$$

$$\text{and } \Delta M^2 = \begin{bmatrix} \Delta m_{41}^2 & 0 & 0 & 0 & 0 \\ 0 & \Delta m_{51}^2 & 0 & 0 & 0 \\ 0 & 0 & \dots & 0 & 0 \\ 0 & 0 & 0 & \dots & 0 \\ 0 & 0 & 0 & 0 & \Delta m_{n1}^2 \end{bmatrix}_{(n-3) \times (n-3)}. \quad (\text{A.3})$$

Here, we assume the magnitude of neutrino masses and their mass-squared splittings are very small compared to their energy (E), i.e., $m_i \ll E$ and $\Delta m_{ij}^2 \ll E$, where i and j are the mass-indices.

An illustration of 3+1 neutrino mixing scenario: By considering $n = 4$, we can introduce a new neutrino, namely sterile neutrino, with mass basis ν_4 and flavor basis ν_s . Using eqs. (A.1) & (A.3), the transition amplitudes in vacuum can be expressed as:

$$\begin{aligned}
& \left(\begin{array}{ccc|c} \langle \nu_e | \nu_e \rangle & \langle \nu_e | \nu_\mu \rangle & \langle \nu_e | \nu_\tau \rangle & \langle \nu_e | \nu_s \rangle \\ \langle \nu_\mu | \nu_e \rangle & \langle \nu_\mu | \nu_\mu \rangle & \langle \nu_\mu | \nu_\tau \rangle & \langle \nu_\mu | \nu_s \rangle \\ \langle \nu_\tau | \nu_e \rangle & \langle \nu_\tau | \nu_\mu \rangle & \langle \nu_\tau | \nu_\tau \rangle & \langle \nu_\tau | \nu_s \rangle \\ \langle \nu_s | \nu_e \rangle & \langle \nu_s | \nu_\mu \rangle & \langle \nu_s | \nu_\tau \rangle & \langle \nu_s | \nu_s \rangle \end{array} \right) = \begin{bmatrix} N & S \\ V & T \end{bmatrix} \begin{bmatrix} e^{-i\frac{\delta m^2}{2E}L} & 0 \\ 0 & e^{-i\frac{\Delta m_{41}^2}{2E}L} \end{bmatrix} \begin{bmatrix} N^\dagger & V^\dagger \\ S^\dagger & T^\dagger \end{bmatrix} \\
& = \left[\begin{array}{c|c} N e^{-i\frac{\delta m^2}{2E}L} N^\dagger + S e^{-i\frac{\Delta m_{41}^2}{2E}L} S^\dagger & N e^{-i\frac{\delta m^2}{2E}L} V^\dagger + S e^{-i\frac{\Delta m_{41}^2}{2E}L} T^\dagger \\ \hline V e^{-i\frac{\delta m^2}{2E}L} N^\dagger + T e^{-i\frac{\Delta m_{41}^2}{2E}L} S^\dagger & V e^{-i\frac{\delta m^2}{2E}L} V^\dagger + T e^{-i\frac{\Delta m_{41}^2}{2E}L} T^\dagger \end{array} \right], \quad (\text{A.4})
\end{aligned}$$

where

$$\begin{pmatrix} N & S \\ V & T \end{pmatrix} = \left(\begin{array}{ccc|c} \tilde{U}_{e1} & \tilde{U}_{e2} & \tilde{U}_{e3} & \tilde{U}_{e4} \\ \tilde{U}_{\mu1} & \tilde{U}_{\mu2} & \tilde{U}_{\mu3} & \tilde{U}_{\mu4} \\ \tilde{U}_{\tau1} & \tilde{U}_{\tau2} & \tilde{U}_{\tau3} & \tilde{U}_{\tau4} \\ \hline \tilde{U}_{s1} & \tilde{U}_{s2} & \tilde{U}_{s3} & \tilde{U}_{s4} \end{array} \right) \text{ and } H_{4 \times 4}^m = \frac{1}{2E} \cdot \begin{bmatrix} \delta m^2 & 0 \\ 0 & \Delta m_{41}^2 \end{bmatrix}. \quad (\text{A.5})$$

With the current knowledge of particle physics and its detection technology, we can not measure the sterile neutrino contents directly. However, using the principle of conservation in neutrino oscillation probabilities, one can infer the impact of such a sterile neutrino. Thus, it is essential to know the information about N , S , δm^2 and Δm_{41}^2 in the 3×3 block of eq. (A.4), to calculate the oscillation probabilities. Now, when $t = 0$, the matrix of transition amplitude becomes an identity one. This gives rise to an important relation for the 3×3 blocks: $N \cdot N^\dagger + S \cdot S^\dagger = I$ and $V \cdot V^\dagger + T \cdot T^\dagger = 1$. In practice, 1×1 block does not provide any useful information because we don't have access to the initial and final states of a sterile neutrino. Now, for a generalized scenario where 'n' number of neutrino species are considered, one may not have all the information regarding either S or ΔM^2 or even both, then only the partial information on the evolution of propagating neutrino will be available via $N e^{-i\frac{\delta m^2}{2E}L} N^\dagger$. Consequently, it gives rise to the non-conservation of three neutrino oscillation probabilities and the corresponding zero-length effect when L has a null value.

Lower-triangular matrix formulation of NUNM: For a generalized neutrino mixing scenario, global unitary mixing matrix $\tilde{U}^{n \times n}$ contains $n(n-1)/2$ number of mixing angles and $(n-2)(n-1)/2$ number of physical phases. Using Okubo's prescription [122], the $\tilde{U}^{n \times n}$ matrix can be constructed with the corresponding $n(n-1)/2$ rotational matrices as:

$$\tilde{U}^{n \times n} = R_{n-1n} \cdot R_{n-2n} \dots R_{3n} \cdot R_{2n} \cdot R_{1n} \dots R_{3n-1} \cdot R_{2n-1} \cdot R_{1n-1} \dots R_{23} \cdot R_{13} \cdot R_{12}. \quad (\text{A.6})$$

While keeping the last three rotational matrices apart from the rest of the matrix multiplications, we can form a lower-triangular matrix. For simplicity, let's consider $n = 4$ which leads to six rotational matrices, and the $\tilde{U}^{4 \times 4}$ can be expressed as:

$$\tilde{U}^{4 \times 4} = R_{34} \cdot R_{24} \cdot R_{14} \cdot R_{23} \cdot R_{13} \cdot R_{12} \quad (\text{A.7})$$

$$= R_{34} \cdot R_{24} \cdot R_{14} \cdot \mathbb{R}, \quad (\text{A.8})$$

where $\mathbb{R} = R_{23} \cdot R_{13} \cdot R_{12}$ and denoting $\sin \theta_{ij}$ ($\cos \theta_{ij}$) = s_{ij} (c_{ij}). For simplicity, considering physical phases to null values

$$R_{34} = \begin{pmatrix} 1 & 0 & 0 & 0 \\ 0 & 1 & 0 & 0 \\ 0 & 0 & c_{34} & -s_{34} \\ 0 & 0 & s_{34} & c_{34} \end{pmatrix}, \quad R_{24} = \begin{pmatrix} 1 & 0 & 0 & 0 \\ 0 & c_{34} & 0 & -s_{34} \\ 0 & 0 & 1 & 0 \\ 0 & s_{34} & 0 & c_{34} \end{pmatrix}, \quad R_{14} = \begin{pmatrix} c_{34} & 0 & 0 & -s_{34} \\ 0 & 1 & 0 & 0 \\ 0 & 0 & 1 & 0 \\ s_{34} & 0 & 0 & c_{34} \end{pmatrix}, \quad (\text{A.9})$$

$$R_{34} \cdot R_{24} \cdot R_{14} = \left(\begin{array}{ccc|c} c_{14} & 0 & 0 & s_{14} \\ -s_{14}s_{24} & c_{24} & 0 & c_{14}s_{24} \\ -c_{24}s_{14}s_{34} & -s_{24}s_{34} & c_{34} & c_{14}c_{24}s_{34} \\ \hline -c_{24}s_{14}c_{34} & -s_{24}s_{34} & -s_{34} & c_{14}c_{24}c_{34} \end{array} \right) \text{ and } \mathbb{R} = \begin{pmatrix} U & 0 \\ 0 & 1 \end{pmatrix}. \quad (\text{A.10})$$

From eqs. (A.8) and (A.10), one can parameterize non-unitary active neutrino mixing matrix N as $N = \alpha \cdot U$, where α is the lower-triangular 3×3 submatrix of $R_{34} \cdot R_{24} \cdot R_{14}$ shown in the above eq. (A.10) and U is standard unitary PMNS matrix.

B Effective ν_μ survival probability in the presence of NUNM

Let us consider an effective two-neutrino scenario in the μ - τ sector, and assigning the vacuum mixing angle θ_{23} and mass-squared splitting as Δm_{32}^2 . Now, considering the new physics scenario of NUNM in 2-3 block and the corresponding oscillation matrix elements

as follows:

$$U = \begin{pmatrix} \cos \theta_{23} & \sin \theta_{23} \\ -\sin \theta_{23} & \cos \theta_{23} \end{pmatrix}, \quad (\text{B.1})$$

$$M = \begin{pmatrix} 0 & 0 \\ 0 & \Delta m_{32}^2 \end{pmatrix}, \quad (\text{B.2})$$

$$\hat{\alpha} = \begin{pmatrix} 1 + \alpha_{22} & 0 \\ \alpha_{32} & 1 + \alpha_{33} \end{pmatrix}, \quad (\text{B.3})$$

$$\begin{aligned} N &= \hat{\alpha} \cdot U \\ &= \begin{pmatrix} 1 + \alpha_{22} & 0 \\ \alpha_{32} & 1 + \alpha_{33} \end{pmatrix} \cdot \begin{pmatrix} \cos \theta_{23} & \sin \theta_{23} \\ -\sin \theta_{23} & \cos \theta_{23} \end{pmatrix}. \end{aligned} \quad (\text{B.4})$$

Now for the simplicity, let us consider $\alpha_{22} = \alpha_{33} = 0$.

$$N = \begin{bmatrix} \cos \theta_{23} & \sin \theta_{23} \\ \alpha_{32} \cos \theta_{23} - \sin \theta_{23} & \cos \theta_{23} + \alpha_{32} \sin \theta_{23} \end{bmatrix}, \quad (\text{B.5})$$

$$\begin{aligned} N^\dagger \cdot V_{NC} \cdot N &= \\ V_{NC} \cdot \begin{bmatrix} c_{23}^2 + (\alpha_{32} c_{23} - s_{23})^2 & c_{23} s_{23} + (\alpha_{32} c_{23} - s_{23})(c_{23} + \alpha_{32} s_{23}) \\ c_{23} s_{23} + (\alpha_{32} c_{23} - s_{23})(c_{23} + \alpha_{32} s_{23}) & s_{23}^2 + (c_{23} + \alpha_{32} s_{23})^2 \end{bmatrix}. \end{aligned} \quad (\text{B.6})$$

The effective Hamiltonian (\mathcal{H}) can be expressed as follows:

$$\mathcal{H} = \frac{M}{2E} + N^\dagger \cdot V_{NC} \cdot N, \quad (\text{B.7})$$

$$\mathcal{H} = V_{NC} \cdot \begin{bmatrix} c_{23}^2 + (\alpha_{32} c_{23} - s_{23})^2 & c_{23} s_{23} + (\alpha_{32} c_{23} - s_{23})(c_{23} + \alpha_{32} s_{23}) \\ c_{23} s_{23} + (\alpha_{32} c_{23} - s_{23})(c_{23} + \alpha_{32} s_{23}) & \Delta m_{32}^2 / 2E V_{NC} + s_{23}^2 + (c_{23} + \alpha_{32} s_{23})^2 \end{bmatrix}. \quad (\text{B.8})$$

The eigenvalues of this effective Hamiltonian, half of the differences of these eigenvalues, will reflect the impact of new physics in the modified oscillation parameters.

$$\lambda_1 = \frac{1}{2} \left[\Delta m_{32}^2/2E + 2V_{NC} + V_{NC}\alpha_{32}^2 - \left\{ (\Delta m_{32}^2/2E)^2 + 4V_{NC}^2\alpha_{32}^2 + V_{NC}^2\alpha_{32}^4 - 2 \cdot \Delta m_{32}^2/2E \cdot V_{NC}\alpha_{32}^2 \cos 2\theta_{23} + 4 \cdot \Delta m_{32}^2/2E \cdot V_{NC}\alpha_{32} \sin 2\theta_{23} \right\}^{1/2} \right], \quad (\text{B.9})$$

$$\lambda_2 = \frac{1}{2} \left[\Delta m_{32}^2/2E + 2V_{NC} + V_{NC}\alpha_{32}^2 + \left\{ (\Delta m_{32}^2/2E)^2 + 4V_{NC}^2\alpha_{32}^2 + V_{NC}^2\alpha_{32}^4 - 2 \cdot \Delta m_{32}^2/2E \cdot V_{NC}\alpha_{32}^2 \cos 2\theta_{23} + 4 \cdot \Delta m_{32}^2/2E \cdot V_{NC}\alpha_{32} \sin 2\theta_{23} \right\}^{1/2} \right], \quad (\text{B.10})$$

$$\frac{\Delta\lambda}{2} = \frac{1}{2} \left\{ (\Delta m_{32}^2/2E)^2 + 4V_{NC}^2\alpha_{32}^2 + V_{NC}^2\alpha_{32}^4 - 2 \cdot \Delta m_{32}^2/2E \cdot V_{NC}\alpha_{32}^2 \cos 2\theta_{23} + 4 \cdot \Delta m_{32}^2/2E \cdot V_{NC}\alpha_{32} \sin 2\theta_{23} \right\}^{1/2}. \quad (\text{B.11})$$

Here, $\Delta\lambda = \lambda_2 - \lambda_1$. Now considering an approximated solution to $\Delta\lambda$ by limiting the higher ordered α_{32}^2 terms $\simeq 0$.

$$\frac{\Delta\lambda}{2} = \frac{1}{2} \left[(\Delta m_{32}^2/2E)^2 + 4 \cdot \Delta m_{32}^2/2E \cdot V_{NC}\alpha_{32} \sin 2\theta_{23} \right]^{1/2}, \quad (\text{B.12})$$

$$\frac{\Delta\lambda}{2} = \Delta m_{32}^2/4E \left[1 + 4 \cdot (\Delta m_{32}^2/2E)^{-1} \cdot V_{NC} \cdot \alpha_{32} \cdot \sin 2\theta_{23} \right]^{1/2}, \quad (\text{B.13})$$

$$\frac{\Delta\lambda}{2} \simeq \Delta m_{32}^2/4E \left[1 + 2 \cdot (\Delta m_{32}^2/2E)^{-1} \cdot V_{NC} \cdot \alpha_{32} \cdot \sin 2\theta_{23} + \dots \right], \quad (\text{B.14})$$

ignoring higher ordered expansion terms of $4 \cdot (\Delta m_{32}^2/2E)^{-1} \cdot V_{NC} \cdot \alpha_{32} \cdot \sin 2\theta_{23}$,

$$\frac{\Delta\lambda}{2} \simeq \frac{\Delta m_{32}^2}{4E} + V_{NC} \cdot \alpha_{32} \cdot \sin 2\theta_{23}, \quad (\text{B.15})$$

$$\boxed{\frac{\Delta\lambda}{2} \cdot L \simeq \left(\frac{\Delta m_{32}^2}{4E} + V_{NC} \cdot \alpha_{32} \cdot \sin 2\theta_{23} \right) \cdot L.} \quad (\text{B.16})$$

Now recalling the $N \cdot N^\dagger$,

$$N \cdot N^\dagger = \begin{pmatrix} 1 & \alpha_{32} \\ \alpha_{32} & 1 + \alpha_{32}^2 \end{pmatrix}, \quad (\text{B.17})$$

$$N \cdot N^\dagger = \begin{bmatrix} (NN^\dagger)_{\mu\mu} & (NN^\dagger)_{\mu\tau} \\ (NN^\dagger)_{\tau\mu} & (NN^\dagger)_{\tau\tau} \end{bmatrix}. \quad (\text{B.18})$$

Thus, $(N \cdot N^\dagger)_{\mu\mu} = 1$,

$$A(\nu_\mu \rightarrow \nu_\mu) = \left(N \cdot e^{-i\mathcal{H}\cdot L} \cdot N^\dagger \right)_{\mu\mu}, \quad (\text{B.19})$$

$$A(\nu_\mu \rightarrow \nu_\mu)(L) = \frac{1}{2} \cdot e^{-i\lambda_1 \cdot L} \cdot \left[\left(1 + e^{i\Delta\lambda \cdot L} \right) - \cos 2\theta_{23} \left(1 - e^{i\Delta\lambda \cdot L} \right) \right]. \quad (\text{B.20})$$

$$P(\nu_\mu \rightarrow \nu_\mu)(L) = \sin^2 2\theta_{23} \cdot \cos^2 \left(\frac{\Delta\lambda}{2} \cdot L \right) + \cos^2 2\theta_{23}, \quad (\text{B.21})$$

$$P(\nu_\mu \rightarrow \nu_\mu)(L) \Big|_{\theta_{23}=\pi/4} = \cos^2 \left(\frac{\Delta\lambda}{2} \cdot L \right), \quad (\text{B.22})$$

$$P(\nu_\mu \rightarrow \nu_\mu)(L) \Big|_{\theta_{23}=\pi/4} = \cos^2 \left[\left(\frac{\Delta m_{32}^2}{4E} + V_{NC} \cdot \alpha_{32} \right) \cdot L \right], \quad (\text{B.23})$$

$$P(\nu_\mu \rightarrow \nu_\mu)(L=0) = \left| (N \cdot N^\dagger)_{\mu\mu} \right|^2 = 1. \quad (\text{B.24})$$

Now accounting for the suppression factor with the NUNM zero-distance effect, i.e., $P_{\text{eff}} = P(L)/P(0)$. Thus, the effective survival oscillation probability of $(\nu_\mu \rightarrow \nu_\mu)$, can be expressed as follows:

$$\boxed{P_{\text{eff}}(\nu_\mu \rightarrow \nu_\mu)(L) \Big|_{\theta_{23}=\pi/4} = \cos^2 \left[\left(\frac{\Delta m_{32}^2}{4E} + V_{NC} \cdot \alpha_{32} \right) \cdot L \right]}. \quad (\text{B.25})$$

C Impact of new physics phase ϕ_{32} on the ν_μ survival probability

In the appendix B, we consider an effective two-neutrino scenario which is insensitive to complex phases, say δ_{CP} and ϕ_{32} . Here, we consider perturbative expansion in the new

physics parameter $|\alpha_{32}|$ and the tri-bi-maximal mixing parameters using the one-mass-scale dominance approximation, i.e., $(\Delta m_{31}^2 L/4E \gg \Delta m_{21}^2 L/4E)$ to derive the expression of ν_μ survival probability in three-neutrino scenario. The tri-bimaximal mixing parameters are defined as: $\sin \theta_{13} = r/\sqrt{3}$, $\sin \theta_{12} = (1-s)/\sqrt{3}$, and $\sin \theta_{23} = (1-a)/\sqrt{2}$. Here, we consider only the impact of $|\alpha_{32}|$ and ϕ_{32} in ν_μ survival channel. The expression upto the second order terms in $|\alpha_{32}|$, r , s , and a is written as:

$$\begin{aligned}
P(\nu_\mu \rightarrow \nu_\mu) \simeq & \cos^2 \Delta_{31} - 2|\alpha_{32}|\Delta_n \sin(2\Delta_{31}) \cos \phi_{32} + \\
& \frac{1}{4\Delta_{31}(\Delta_{31} - \Delta_e)^2} \times \left[\Delta_{31} \left\{ 2r^2 \Delta_{31}^2 \cos \Delta_{31} \cos(\Delta_{31} - 2\Delta_e) \right. \right. \\
& \left. \left. - r^2 \Delta_{31}^2 + 8a^2(\Delta_{31} - \Delta_e)^2 \right\} - \Delta_{31} \cos 2\Delta_{31} \left\{ r^2 \Delta_{31}^2 + 8a^2(\Delta_{31} - \Delta_e)^2 \right. \right. \\
& \left. \left. + 16|\alpha_{32}|^2(\Delta_{31} - \Delta_e)^2 \Delta_n^2 \cos^2 \phi_{32} \right\} - 2(\Delta_{31} - \Delta_e) \left\{ r^2 \Delta_{31}^2 \Delta_e \right. \right. \\
& \left. \left. + 4|\alpha_{32}|^2(\Delta_{31} - \Delta_e)\Delta_n^2 \sin^2 \phi_{32} \right\} \sin(2\Delta_{31}) \right], \tag{C.1}
\end{aligned}$$

where $\Delta_{31} = \Delta m_{31}^2 L/4E$, $\Delta_e = G_F N_e L/\sqrt{2}$, and $\Delta_n = -G_F N_n L/2\sqrt{2}$. Here, the terms associated with δ_{CP} , i.e., α_{21} and α_{31} are considered to be zero [123]. Therefore, at the leading order terms, the oscillation probability of ν_μ survival channel is almost insensitive to δ_{CP} , and the impact of the new physics parameter drop down to real value of α_{32} .

References

- [1] **Particle Data Group** Collaboration, R. L. Workman and Others, *Review of Particle Physics*, *PTEP* **2022** (2022) 083C01.
- [2] **Super-Kamiokande** Collaboration, Y. Fukuda et al., *Constraints on neutrino oscillation parameters from the measurement of day night solar neutrino fluxes at Super-Kamiokande*, *Phys. Rev. Lett.* **82** (1999) 1810–1814, [[hep-ex/9812009](#)].
- [3] **Super-Kamiokande** Collaboration, S. Fukuda et al., *Constraints on neutrino oscillations using 1258 days of Super-Kamiokande solar neutrino data*, *Phys. Rev. Lett.* **86** (2001) 5656–5660, [[hep-ex/0103033](#)].
- [4] **SNO** Collaboration, Q. R. Ahmad et al., *Measurement of the rate of $\nu_e + d \rightarrow p + p + e^-$ interactions produced by ^8B solar neutrinos at the Sudbury Neutrino Observatory*, *Phys. Rev. Lett.* **87** (2001) 071301, [[nucl-ex/0106015](#)].
- [5] **Super-Kamiokande** Collaboration, S. Fukuda et al., *Determination of solar neutrino oscillation parameters using 1496 days of Super-Kamiokande I data*, *Phys. Lett. B* **539** (2002) 179–187, [[hep-ex/0205075](#)].
- [6] **Super-Kamiokande** Collaboration, J. Hosaka et al., *Solar neutrino measurements in super-Kamiokande-I*, *Phys. Rev. D* **73** (2006) 112001, [[hep-ex/0508053](#)].
- [7] **Super-Kamiokande** Collaboration, J. P. Cravens et al., *Solar neutrino measurements in Super-Kamiokande-II*, *Phys. Rev. D* **78** (2008) 032002, [[arXiv:0803.4312](#)].
- [8] **Super-Kamiokande** Collaboration, K. Abe et al., *Solar neutrino results in Super-Kamiokande-III*, *Phys. Rev. D* **83** (2011) 052010, [[arXiv:1010.0118](#)].

- [9] **SNO** Collaboration, B. Aharmim et al., *Combined Analysis of all Three Phases of Solar Neutrino Data from the Sudbury Neutrino Observatory*, *Phys. Rev. C* **88** (2013) 025501, [[arXiv:1109.0763](#)].
- [10] **KamLAND** Collaboration, K. Eguchi et al., *First results from KamLAND: Evidence for reactor anti-neutrino disappearance*, *Phys. Rev. Lett.* **90** (2003) 021802, [[hep-ex/0212021](#)].
- [11] **KamLAND Collaboration** Collaboration, T. Araki et al., *Measurement of neutrino oscillation with KamLAND: Evidence of spectral distortion*, *Phys.Rev.Lett.* **94** (2005) 081801, [[hep-ex/0406035](#)].
- [12] **Daya Bay** Collaboration, F. P. An et al., *Observation of electron-antineutrino disappearance at Daya Bay*, *Phys. Rev. Lett.* **108** (2012) 171803, [[arXiv:1203.1669](#)].
- [13] **RENO** Collaboration, J. K. Ahn et al., *Observation of Reactor Electron Antineutrino Disappearance in the RENO Experiment*, *Phys. Rev. Lett.* **108** (2012) 191802, [[arXiv:1204.0626](#)].
- [14] **KamLAND** Collaboration, A. Gando et al., *Reactor On-Off Antineutrino Measurement with KamLAND*, *Phys. Rev. D* **88** (2013), no. 3 033001, [[arXiv:1303.4667](#)].
- [15] **RENO** Collaboration, G. Bak et al., *Measurement of Reactor Antineutrino Oscillation Amplitude and Frequency at RENO*, *Phys. Rev. Lett.* **121** (2018), no. 20 201801, [[arXiv:1806.00248](#)].
- [16] **Daya Bay** Collaboration, D. Adey et al., *Measurement of the Electron Antineutrino Oscillation with 1958 Days of Operation at Daya Bay*, *Phys. Rev. Lett.* **121** (2018), no. 24 241805, [[arXiv:1809.02261](#)].
- [17] **Double Chooz** Collaboration, H. de Kerret et al., *Double Chooz θ_{13} measurement via total neutron capture detection*, *Nature Phys.* **16** (2020), no. 5 558–564, [[arXiv:1901.09445](#)].
- [18] C. V. Achar et al., *Detection of muons produced by cosmic ray neutrinos deep underground*, *Phys. Lett.* **18** (1965) 196–199.
- [19] **Super-Kamiokande** Collaboration, Y. Fukuda et al., *Evidence for oscillation of atmospheric neutrinos*, *Phys. Rev. Lett.* **81** (1998) 1562, [[hep-ex/9807003](#)].
- [20] **Super-Kamiokande** Collaboration, Y. Ashie et al., *Evidence for an oscillatory signature in atmospheric neutrino oscillation*, *Phys. Rev. Lett.* **93** (2004) 101801, [[hep-ex/0404034](#)].
- [21] **IceCube** Collaboration, M. G. Aartsen et al., *Determining neutrino oscillation parameters from atmospheric muon neutrino disappearance with three years of IceCube DeepCore data*, *Phys. Rev. D* **91** (2015), no. 7 072004, [[arXiv:1410.7227](#)].
- [22] **Super-Kamiokande** Collaboration, K. Abe et al., *Atmospheric neutrino oscillation analysis with external constraints in Super-Kamiokande I-IV*, *Phys. Rev. D* **97** (2018), no. 7 072001, [[arXiv:1710.09126](#)].
- [23] **K2K** Collaboration, E. Aliu et al., *Evidence for muon neutrino oscillation in an accelerator-based experiment*, *Phys. Rev. Lett.* **94** (2005) 081802, [[hep-ex/0411038](#)].
- [24] **MINOS** Collaboration, P. Adamson et al., *Measurement of Neutrino Oscillations with the MINOS Detectors in the NuMI Beam*, *Phys.Rev.Lett.* **101** (2008) 131802, [[arXiv:0806.2237](#)].
- [25] **MINOS** Collaboration, P. Adamson et al., *Electron neutrino and antineutrino appearance*

- in the full MINOS data sample, *Phys. Rev. Lett.* **110** (2013), no. 17 171801, [[arXiv:1301.4581](#)].
- [26] **MINOS** Collaboration, P. Adamson et al., *Measurement of Neutrino and Antineutrino Oscillations Using Beam and Atmospheric Data in MINOS*, *Phys. Rev. Lett.* **110** (2013), no. 25 251801, [[arXiv:1304.6335](#)].
- [27] **T2K** Collaboration, K. Abe et al., *Constraint on the matter–antimatter symmetry-violating phase in neutrino oscillations*, *Nature* **580** (2020), no. 7803 339–344, [[arXiv:1910.03887](#)]. [Erratum: *Nature* 583, E16 (2020)].
- [28] **NOvA** Collaboration, M. A. Acero et al., *First Measurement of Neutrino Oscillation Parameters using Neutrinos and Antineutrinos by NOvA*, *Phys. Rev. Lett.* **123** (2019), no. 15 151803, [[arXiv:1906.04907](#)].
- [29] T. Kajita, *Nobel Lecture: Discovery of atmospheric neutrino oscillations*, *Rev. Mod. Phys.* **88** (2016), no. 3 030501.
- [30] A. B. McDonald, *Nobel Lecture: The Sudbury Neutrino Observatory: Observation of flavor change for solar neutrinos*, *Rev. Mod. Phys.* **88** (2016), no. 3 030502.
- [31] **SLD Electroweak Group, DELPHI, ALEPH, SLD, SLD Heavy Flavour Group, OPAL, LEP Electroweak Working Group, L3** Collaboration, S. Schael et al., *Precision electroweak measurements on the Z resonance*, *Phys. Rept.* **427** (2006) 257–454, [[hep-ex/0509008](#)].
- [32] **LSND** Collaboration, C. Athanassopoulos et al., *Candidate events in a search for muon antineutrino to electron antineutrino oscillations*, *Phys. Rev. Lett.* **75** (1995) 2650–2653, [[nucl-ex/9504002](#)].
- [33] **LSND** Collaboration, A. Aguilar-Arevalo et al., *Evidence for neutrino oscillations from the observation of $\bar{\nu}_e$ appearance in a $\bar{\nu}_\mu$ beam*, *Phys. Rev. D* **64** (2001) 112007, [[hep-ex/0104049](#)].
- [34] **MiniBooNE** Collaboration, A. A. Aguilar-Arevalo et al., *A Search for Electron Neutrino Appearance at the $\Delta m^2 \sim 1\text{eV}^2$ Scale*, *Phys. Rev. Lett.* **98** (2007) 231801, [[arXiv:0704.1500](#)].
- [35] **MiniBooNE** Collaboration, A. A. Aguilar-Arevalo et al., *Event Excess in the MiniBooNE Search for $\bar{\nu}_\mu \rightarrow \bar{\nu}_e$ Oscillations*, *Phys. Rev. Lett.* **105** (2010) 181801, [[arXiv:1007.1150](#)].
- [36] F. Kaether, W. Hampel, G. Heusser, J. Kiko, and T. Kirsten, *Reanalysis of the GALLEX solar neutrino flux and source experiments*, *Phys. Lett.* **B685** (2010) 47–54, [[arXiv:1001.2731](#)].
- [37] **SAGE** Collaboration, J. N. Abdurashitov et al., *Measurement of the solar neutrino capture rate with gallium metal. III: Results for the 2002–2007 data-taking period*, *Phys. Rev.* **C80** (2009) 015807, [[arXiv:0901.2200](#)].
- [38] V. V. Barinov et al., *Search for electron-neutrino transitions to sterile states in the BEST experiment*, *Phys. Rev. C* **105** (2022), no. 6 065502, [[arXiv:2201.07364](#)].
- [39] **NEUTRINO-4** Collaboration, A. P. Serebrov et al., *First Observation of the Oscillation Effect in the Neutrino-4 Experiment on the Search for the Sterile Neutrino*, *Pisma Zh. Eksp. Teor. Fiz.* **109** (2019), no. 4 209–218, [[arXiv:1809.10561](#)].
- [40] A. Boyarsky, O. Ruchayskiy, D. Iakubovskiy, and J. Franse, *Unidentified Line in X-Ray*

- Spectra of the Andromeda Galaxy and Perseus Galaxy Cluster*, *Phys. Rev. Lett.* **113** (2014) 251301, [[arXiv:1402.4119](#)].
- [41] E. Bulbul, M. Markevitch, A. Foster, R. K. Smith, M. Loewenstein, and S. W. Randall, *Detection of An Unidentified Emission Line in the Stacked X-ray spectrum of Galaxy Clusters*, *Astrophys. J.* **789** (2014) 13, [[arXiv:1402.2301](#)].
- [42] A. Abada, G. Arcadi, and M. Lucente, *Dark Matter in the minimal Inverse Seesaw mechanism*, *JCAP* **10** (2014) 001, [[arXiv:1406.6556](#)].
- [43] K. N. Abazajian, *Resonantly Produced 7 keV Sterile Neutrino Dark Matter Models and the Properties of Milky Way Satellites*, *Phys. Rev. Lett.* **112** (2014), no. 16 161303, [[arXiv:1403.0954](#)].
- [44] K. C. Y. Ng, S. Horiuchi, J. M. Gaskins, M. Smith, and R. Preece, *Improved Limits on Sterile Neutrino Dark Matter using Full-Sky Fermi Gamma-Ray Burst Monitor Data*, *Phys. Rev. D* **92** (2015), no. 4 043503, [[arXiv:1504.04027](#)].
- [45] A. Schneider, *Astrophysical constraints on resonantly produced sterile neutrino dark matter*, *JCAP* (2016) 059, [[arXiv:1601.07553](#)].
- [46] S. Weinberg, *Baryon and Lepton Nonconserving Processes*, *Phys. Rev. Lett.* **43** (1979) 1566–1570.
- [47] S. Weinberg, *Varieties of Baryon and Lepton Nonconservation*, *Phys. Rev. D* **22** (1980) 1694.
- [48] P. Minkowski, *$\mu \rightarrow e\gamma$ at a Rate of One Out of 10^9 Muon Decays?*, *Phys. Lett. B* **67** (1977) 421–428.
- [49] T. Yanagida, *Horizontal gauge symmetry and masses of neutrinos*, *Conf. Proc. C* **7902131** (1979) 95–99.
- [50] M. Gell-Mann, P. Ramond, and R. Slansky, *Complex Spinors and Unified Theories*, *Conf. Proc. C* **790927** (1979) 315–321, [[arXiv:1306.4669](#)].
- [51] P. Ramond, *The Family Group in Grand Unified Theories*, in *International Symposium on Fundamentals of Quantum Theory and Quantum Field Theory*, 2, 1979. [hep-ph/9809459](#).
- [52] T. Yanagida, *Horizontal Symmetry and Masses of Neutrinos*, *Prog. Theor. Phys.* **64** (1980) 1103.
- [53] J. Schechter and J. W. F. Valle, *Neutrino Masses in $SU(2) \times U(1)$ Theories*, *Phys. Rev. D* **22** (1980) 2227.
- [54] R. N. Mohapatra and G. Senjanovic, *Neutrino Masses and Mixings in Gauge Models with Spontaneous Parity Violation*, *Phys. Rev. D* **23** (1981) 165.
- [55] J. Schechter and J. W. F. Valle, *Neutrino Decay and Spontaneous Violation of Lepton Number*, *Phys. Rev. D* **25** (1982) 774.
- [56] E. Ma, *Pathways to naturally small neutrino masses*, *Phys. Rev. Lett.* **81** (1998) 1171–1174, [[hep-ph/9805219](#)].
- [57] S. Antusch, C. Biggio, E. Fernandez-Martinez, M. B. Gavela, and J. Lopez-Pavon, *Unitarity of the Leptonic Mixing Matrix*, *JHEP* **10** (2006) 084, [[hep-ph/0607020](#)].
- [58] S. Antusch, M. Blennow, E. Fernandez-Martinez, and J. Lopez-Pavon, *Probing non-unitary mixing and CP-violation at a Neutrino Factory*, *Phys.Rev.* **D80** (2009) 033002, [[arXiv:0903.3986](#)].

- [59] F. J. Escrihuela, D. V. Forero, O. G. Miranda, M. Tortola, and J. W. F. Valle, *On the description of nonunitary neutrino mixing*, *Phys. Rev. D* **92** (2015), no. 5 053009, [[arXiv:1503.08879](#)]. [Erratum: *Phys.Rev.D* 93, 119905 (2016)].
- [60] C. S. Fong, H. Minakata, and H. Nunokawa, *Non-unitary evolution of neutrinos in matter and the leptonic unitarity test*, *JHEP* **02** (2019) 015, [[arXiv:1712.02798](#)].
- [61] **ICAL** Collaboration, S. Ahmed et al., *Physics Potential of the ICAL detector at the India-based Neutrino Observatory (INO)*, *Pramana* **88** (2017), no. 5 79, [[arXiv:1505.07380](#)].
- [62] S. P. Behera, M. S. Bhatia, V. M. Datar, and A. K. Mohanty, *Simulation Studies for Electromagnetic Design of INO ICAL Magnet and its Response to Muons*, *IEEE Trans. Magnetics* **51** (2015) 4624, [[arXiv:1406.3965](#)].
- [63] M. M. Devi, T. Thakore, S. K. Agarwalla, and A. Dighe, *Enhancing sensitivity to neutrino parameters at INO combining muon and hadron information*, *JHEP* **10** (2014) 189, [[arXiv:1406.3689](#)].
- [64] A. Chatterjee, K. Meghna, K. Rawat, T. Thakore, V. Bhatnagar, et al., *A Simulations Study of the Muon Response of the Iron Calorimeter Detector at the India-based Neutrino Observatory*, *JINST* **9** (2014) P07001, [[arXiv:1405.7243](#)].
- [65] M. M. Devi, A. Ghosh, D. Kaur, L. S. Mohan, S. Choubey, et al., *Hadron energy response of the Iron Calorimeter detector at the India-based Neutrino Observatory*, *JINST* **8** (2013) P11003, [[arXiv:1304.5115](#)].
- [66] S. Goswami, *Physics program of india based neutrino observatory*, *Nuclear Physics B - Proceedings Supplements* **188** (2009) 198–200. Proceedings of the Neutrino Oscillation Workshop.
- [67] A. Ghosh, T. Thakore, and S. Choubey, *Determining the Neutrino Mass Hierarchy with INO, T2K, NOvA and Reactor Experiments*, *JHEP* **1304** (2013) 009, [[arXiv:1212.1305](#)].
- [68] T. Thakore, A. Ghosh, S. Choubey, and A. Dighe, *The Reach of INO for Atmospheric Neutrino Oscillation Parameters*, *JHEP* **1305** (2013) 058, [[arXiv:1303.2534](#)].
- [69] A. Ghosh and S. Choubey, *Measuring the Mass Hierarchy with Muon and Hadron Events in Atmospheric Neutrino Experiments*, *JHEP* **1310** (2013) 174, [[arXiv:1306.1423](#)].
- [70] N. Dash, V. M. Datar, and G. Majumder, *Sensitivity of the INO-ICAL detector to magnetic monopoles*, *Astropart. Phys.* **70** (2015) 33–38, [[arXiv:1406.3938](#)].
- [71] A. Chatterjee, R. Gandhi, and J. Singh, *Probing Lorentz and CPT Violation in a Magnetized Iron Detector using Atmospheric Neutrinos*, *JHEP* **1406** (2014) 045, [[arXiv:1402.6265](#)].
- [72] S. Choubey, A. Ghosh, T. Ohlsson, and D. Tiwari, *Neutrino Physics with Non-Standard Interactions at INO*, *JHEP* **12** (2015) 126, [[arXiv:1507.02211](#)].
- [73] L. S. Mohan and D. Indumathi, *Pinning down neutrino oscillation parameters in the 2–3 sector with a magnetised atmospheric neutrino detector: a new study*, *Eur. Phys. J.* **C77** (2017), no. 1 54, [[arXiv:1605.04185](#)].
- [74] S. P. Behera, A. Ghosh, S. Choubey, V. M. Datar, D. K. Mishra, and A. K. Mohanty, *Search for the sterile neutrino mixing with the ICAL detector at INO*, *Eur. Phys. J.* **C77** (2017), no. 5 307, [[arXiv:1605.08607](#)].

- [75] A. Khatun, R. Laha, and S. K. Agarwalla, *Indirect searches of Galactic diffuse dark matter in INO-MagICAL detector*, *JHEP* **06** (2017) 057, [[arXiv:1703.10221](#)].
- [76] S. Choubey, A. Ghosh, and D. Tiwari, *Prospects of Indirect Searches for Dark Matter at INO*, *JCAP* **05** (2018) 006, [[arXiv:1711.02546](#)].
- [77] S. Choubey, S. Goswami, C. Gupta, S. M. Lakshmi, and T. Thakore, *Sensitivity to neutrino decay with atmospheric neutrinos at the INO-ICAL detector*, *Phys. Rev. D* **97** (2018), no. 3 033005, [[arXiv:1709.10376](#)].
- [78] D. Kaur, Z. A. Dar, S. Kumar, and M. Naimuddin, *Search for the differences in atmospheric neutrino and antineutrino oscillation parameters at the INO-ICAL experiment*, *Phys. Rev. D* **95** (2017), no. 9 093005, [[arXiv:1703.06710](#)].
- [79] K. R. Rebin, J. Libby, D. Indumathi, and L. S. Mohan, *Study of neutrino oscillation parameters at the INO-ICAL detector using event-by-event reconstruction*, *Eur. Phys. J. C* **79** (2019), no. 4 295, [[arXiv:1804.02138](#)].
- [80] T. Thakore, M. M. Devi, S. K. Agarwalla, and A. Dighe, *Active-sterile neutrino oscillations at INO-ICAL over a wide mass-squared range*, *JHEP* **08** (2018) 022, [[arXiv:1804.09613](#)].
- [81] A. Khatun, T. Thakore, and S. K. Agarwalla, *Can INO be Sensitive to Flavor-Dependent Long-Range Forces?*, *JHEP* **04** (2018) 023, [[arXiv:1801.00949](#)].
- [82] D. Tiwari, S. Choubey, and A. Ghosh, *Prospects of indirect searches for dark matter annihilations in the earth with ICAL@INO*, *JHEP* **05** (2019) 039, [[arXiv:1806.05058](#)].
- [83] J. Datta, M. Nizam, A. Ajmi, and S. U. Sankar, *Matter vs vacuum oscillations in atmospheric neutrinos*, *Nucl. Phys. B* **961** (2020) 115251, [[arXiv:1907.08966](#)].
- [84] Z. A. Dar, D. Kaur, S. Kumar, and M. Naimuddin, *Independent measurement of muon neutrino and antineutrino oscillations at the INO-ICAL experiment*, *J. Phys. G* **46** (2019), no. 6 065001, [[arXiv:2004.01127](#)].
- [85] A. Khatun, S. S. Chatterjee, T. Thakore, and S. K. Agarwalla, *Enhancing sensitivity to non-standard neutrino interactions at INO combining muon and hadron information*, *Eur. Phys. J. C* **80** (2020), no. 6 533, [[arXiv:1907.02027](#)].
- [86] A. Kumar, A. Khatun, S. K. Agarwalla, and A. Dighe, *From oscillation dip to oscillation valley in atmospheric neutrino experiments*, *Eur. Phys. J. C* **81** (2021), no. 2 190, [[arXiv:2006.14529](#)].
- [87] A. Kumar and S. K. Agarwalla, *Validating the Earth's core using atmospheric neutrinos with ICAL at INO*, *JHEP* **08** (2021) 139, [[arXiv:2104.11740](#)].
- [88] A. Kumar, A. Khatun, S. K. Agarwalla, and A. Dighe, *A New Approach to Probe Non-Standard Interactions in Atmospheric Neutrino Experiments*, *JHEP* **04** (2021) 159, [[arXiv:2101.02607](#)].
- [89] S. Sahoo, A. Kumar, and S. K. Agarwalla, *Probing Lorentz Invariance Violation with atmospheric neutrinos at INO-ICAL*, *JHEP* **03** (2022) 050, [[arXiv:2110.13207](#)].
- [90] S. Sahoo, A. Kumar, and S. K. Agarwalla, *Exploring the Violation of Lorentz Invariance using Atmospheric Neutrinos at INO-ICAL*, *J. Phys. Conf. Ser.* **2156** (2021) 012238.
- [91] A. K. Upadhyay, A. Kumar, S. K. Agarwalla, and A. Dighe, *Neutrino oscillations in Earth for probing dark matter inside the core*, [arXiv:2112.14201](#).

- [92] S. Sahoo, A. Kumar, S. K. Agarwalla, and A. Dighe, *Core-passing atmospheric neutrinos: a unique probe to discriminate between Lorentz violation and non-standard interactions*, [arXiv:2205.05134](#).
- [93] R. T. Senthil, D. Indumathi, and P. Shukla, *Simulation study of tau neutrino events at the ICAL detector in INO*, *Phys. Rev. D* **106** (2022), no. 9 093004, [[arXiv:2203.09863](#)].
- [94] A. K. Upadhyay, A. Kumar, S. K. Agarwalla, and A. Dighe, *Locating the Core-Mantle Boundary using Oscillations of Atmospheric Neutrinos*, [arXiv:2211.08688](#).
- [95] D. Raikwal, S. Choubey, and M. Ghosh, *Determining neutrino mass ordering with ICAL, JUNO and T2HK*, *Eur. Phys. J. Plus* **138** (2023), no. 2 110, [[arXiv:2207.06798](#)].
- [96] D. Raikwal, S. Choubey, and M. Ghosh, *Comprehensive study of LIV in atmospheric and long-baseline experiments*, [arXiv:2303.10892](#).
- [97] **DUNE** Collaboration, R. Acciarri et al., *Long-Baseline Neutrino Facility (LBNF) and Deep Underground Neutrino Experiment (DUNE): Conceptual Design Report, Volume 2: The Physics Program for DUNE at LBNF*, [arXiv:1512.06148](#).
- [98] **DUNE** Collaboration, B. Abi et al., *Deep Underground Neutrino Experiment (DUNE), Far Detector Technical Design Report, Volume I Introduction to DUNE*, *JINST* **15** (2020), no. 08 T08008, [[arXiv:2002.02967](#)].
- [99] **DUNE** Collaboration, B. Abi et al., *Deep Underground Neutrino Experiment (DUNE), Far Detector Technical Design Report, Volume II: DUNE Physics*, [arXiv:2002.03005](#).
- [100] **DUNE** Collaboration, B. Abi et al., *Long-baseline neutrino oscillation physics potential of the DUNE experiment*, *Eur. Phys. J. C* **80** (2020), no. 10 978, [[arXiv:2006.16043](#)].
- [101] **DUNE** Collaboration, B. Abi et al., *Prospects for beyond the Standard Model physics searches at the Deep Underground Neutrino Experiment*, *Eur. Phys. J. C* **81** (2021), no. 4 322, [[arXiv:2008.12769](#)].
- [102] **DUNE** Collaboration, A. Abud Abed et al., *Low exposure long-baseline neutrino oscillation sensitivity of the DUNE experiment*, *Phys. Rev. D* **105** (2022), no. 7 072006, [[arXiv:2109.01304](#)].
- [103] **DUNE** Collaboration, B. Abi et al., *Experiment Simulation Configurations Approximating DUNE TDR*, [arXiv:2103.04797](#).
- [104] **Hyper-Kamiokande** Collaboration, K. Abe et al., *Physics potentials with the second Hyper-Kamiokande detector in Korea*, *PTEP* **2018** (2018), no. 6 063C01, [[arXiv:1611.06118](#)].
- [105] **Hyper-Kamiokande** Collaboration, K. Abe et al., *Hyper-Kamiokande Design Report*, [arXiv:1805.04163](#).
- [106] B. Pontecorvo, *Inverse beta processes and nonconservation of lepton charge*, *Zh. Eksp. Teor. Fiz.* **34** (1957) 247.
- [107] B. Pontecorvo, *Neutrino Experiments and the Problem of Conservation of Leptonic Charge*, *Zh. Eksp. Teor. Fiz.* **53** (1967) 1717–1725.
- [108] Z. Maki, M. Nakagawa, and S. Sakata, *Remarks on the unified model of elementary particles*, *Prog. Theor. Phys.* **28** (1962) 870–880.
- [109] C. Giunti, *Neutrino wave packets in quantum field theory*, *JHEP* **11** (2002) 017, [[hep-ph/0205014](#)].

- [110] C. Giunti and C. W. Kim, *Fundamentals of Neutrino Physics and Astrophysics*. Oxford University Press, 2007.
- [111] E. K. Akhmedov and A. Y. Smirnov, *Paradoxes of neutrino oscillations*, *Phys. Atom. Nucl.* **72** (2009) 1363–1381, [[arXiv:0905.1903](#)].
- [112] E. Akhmedov, *Quantum mechanics aspects and subtleties of neutrino oscillations*, in *International Conference on History of the Neutrino: 1930-2018*, 1, 2019. [[arXiv:1901.05232](#)].
- [113] J. Sato, *Neutrino oscillation and CP violation*, *Nucl. Instrum. Meth. A* **472** (2001) 434–439, [[hep-ph/0008056](#)].
- [114] H. Nunokawa, S. J. Parke, and J. W. F. Valle, *CP Violation and Neutrino Oscillations*, *Prog. Part. Nucl. Phys.* **60** (2008) 338–402, [[arXiv:0710.0554](#)].
- [115] H. Hettmansperger, M. Lindner, and W. Rodejohann, *Phenomenological Consequences of sub-leading Terms in See-Saw Formulas*, *JHEP* **04** (2011) 123, [[arXiv:1102.3432](#)].
- [116] C. S. Fong, *Theoretical Aspect of Nonunitarity in Neutrino Oscillation*, [[arXiv:2301.12960](#)].
- [117] Z.-z. Xing, *Towards testing the unitarity of the 3×3 lepton flavor mixing matrix in a precision reactor antineutrino oscillation experiment*, *Phys. Lett. B* **718** (2013) 1447–1453, [[arXiv:1210.1523](#)].
- [118] K. Bielas, W. Flieger, J. Gluza, and M. Gluza, *Neutrino mixing, interval matrices and singular values*, *Phys. Rev. D* **98** (2018), no. 5 053001, [[arXiv:1708.09196](#)].
- [119] W. Flieger, J. Gluza, and K. Porwit, *New limits on neutrino non-unitary mixings based on prescribed singular values*, *JHEP* **03** (2020) 169, [[arXiv:1910.01233](#)].
- [120] S. A. R. Ellis, K. J. Kelly, and S. W. Li, *Leptonic Unitarity Triangles*, *Phys. Rev. D* **102** (2020), no. 11 115027, [[arXiv:2004.13719](#)].
- [121] Z. Hu, J. Ling, J. Tang, and T. Wang, *Global oscillation data analysis on the 3ν mixing without unitarity*, *JHEP* **01** (2021) 124, [[arXiv:2008.09730](#)].
- [122] S. Okubo, *Note on Unitary Symmetry in Strong Interaction. II Excited States of Baryons*, *Prog. Theor. Phys.* **28** (1962) 24–32.
- [123] S. K. Agarwalla, S. Das, A. Giarnetti, and D. Meloni, *Model-independent constraints on non-unitary neutrino mixing from high-precision long-baseline experiments*, *JHEP* **07** (2022) 121, [[arXiv:2111.00329](#)].
- [124] S. Gariazzo, P. Martínez-Miravé, O. Mena, S. Pastor, and M. Tórtola, *Non-unitary three-neutrino mixing in the early Universe*, *JCAP* **03** (2023) 046, [[arXiv:2211.10522](#)].
- [125] C. A. Argüelles et al., *Snowmass white paper: beyond the standard model effects on neutrino flavor: Submitted to the proceedings of the US community study on the future of particle physics (Snowmass 2021)*, *Eur. Phys. J. C* **83** (2023), no. 1 15, [[arXiv:2203.10811](#)].
- [126] M. Blennow, P. Coloma, E. Fernandez-Martinez, J. Hernandez-Garcia, and J. Lopez-Pavon, *Non-Unitarity, sterile neutrinos, and Non-Standard neutrino Interactions*, *JHEP* **04** (2017) 153, [[arXiv:1609.08637](#)].
- [127] L. S. Miranda, P. Pasquini, U. Rahaman, and S. Razzaque, *Searching for non-unitary neutrino oscillations in the present T2K and NO ν A data*, *Eur. Phys. J. C* **81** (2021), no. 5 444, [[arXiv:1911.09398](#)].

- [128] D. V. Forero, C. Giunti, C. A. Ternes, and M. Tortola, *Nonunitary neutrino mixing in short and long-baseline experiments*, *Phys. Rev. D* **104** (2021), no. 7 075030, [[arXiv:2103.01998](#)].
- [129] M. Blennow, E. Fernández-Martínez, J. Hernández-García, J. López-Pavón, X. Marcano, and D. Naredo-Tuero, *Bounds on lepton non-unitarity and heavy neutrino mixing*, *JHEP* **08** (2023) 030, [[arXiv:2306.01040](#)].
- [130] **NOMAD** Collaboration, P. Astier et al., *Final NOMAD results on muon-neutrino \rightarrow tau-neutrino and electron-neutrino \rightarrow tau-neutrino oscillations including a new search for tau-neutrino appearance using hadronic tau decays*, *Nucl. Phys. B* **611** (2001) 3–39, [[hep-ex/0106102](#)].
- [131] **NOMAD** Collaboration, P. Astier et al., *Search for $\nu(\mu) \rightarrow \nu(e)$ oscillations in the NOMAD experiment*, *Phys. Lett. B* **570** (2003) 19–31, [[hep-ex/0306037](#)].
- [132] S.-F. Ge, P. Pasquini, M. Tortola, and J. W. F. Valle, *Measuring the leptonic CP phase in neutrino oscillations with nonunitary mixing*, *Phys. Rev. D* **95** (2017), no. 3 033005, [[arXiv:1605.01670](#)].
- [133] **MINOS** Collaboration, P. Adamson et al., *Search for Sterile Neutrinos Mixing with Muon Neutrinos in MINOS*, *Phys. Rev. Lett.* **117** (2016), no. 15 151803, [[arXiv:1607.01176](#)].
- [134] **Super-Kamiokande** Collaboration, K. Abe et al., *Limits on sterile neutrino mixing using atmospheric neutrinos in Super-Kamiokande*, *Phys. Rev. D* **91** (2015) 052019, [[arXiv:1410.2008](#)].
- [135] **Hyper-Kamiokande Proto-Collaboration** Collaboration, K. Abe et al., *Physics potential of a long-baseline neutrino oscillation experiment using a J-PARC neutrino beam and Hyper-Kamiokande*, *PTEP* **2015** (2015) 053C02, [[arXiv:1502.05199](#)].
- [136] F. Capozzi, C. Giunti, and C. A. Ternes, *Improved sensitivities of $ESS\nu SB$ from a two-detector fit*, *JHEP* **04** (2023) 130, [[arXiv:2302.07154](#)].
- [137] J. M. Celestino-Ramírez, F. J. Escrihuela, L. J. Flores, and O. G. Miranda, *Testing the nonunitarity of the leptonic mixing matrix at FASER ν and FASER $\nu 2$* , *Phys. Rev. D* **109** (2024), no. 1 L011705, [[arXiv:2309.00116](#)].
- [138] **OPERA** Collaboration, N. Agafonova et al., *Final Results of the OPERA Experiment on ν_τ Appearance in the CNGS Neutrino Beam*, *Phys. Rev. Lett.* **120** (2018), no. 21 211801, [[arXiv:1804.04912](#)]. [Erratum: *Phys.Rev.Lett.* 121, 139901 (2018)].
- [139] **Super-Kamiokande** Collaboration, Z. Li et al., *Measurement of the tau neutrino cross section in atmospheric neutrino oscillations with Super-Kamiokande*, *Phys. Rev. D* **98** (2018), no. 5 052006, [[arXiv:1711.09436](#)].
- [140] **IceCube** Collaboration, M. G. Aartsen et al., *Measurement of Atmospheric Tau Neutrino Appearance with IceCube DeepCore*, *Phys. Rev. D* **99** (2019), no. 3 032007, [[arXiv:1901.05366](#)].
- [141] **KM3NeT** Collaboration, N. Geislbrecht, *First measurement of tau appearance with KM3NeT/ORCA6*, *PoS ICRC2023* (2023) 1107.
- [142] **IceCube** Collaboration, R. Abbasi et al., *Detection of astrophysical tau neutrino candidates in IceCube*, *Eur. Phys. J. C* **82** (2022), no. 11 1031, [[arXiv:2011.03561](#)].
- [143] **IceCube** Collaboration, R. Abbasi et al., *Summary of IceCube tau neutrino searches and flavor composition measurements of the diffuse astrophysical neutrino flux*, *PoS ICRC2023* (2023) 1122, [[arXiv:2308.15213](#)].

- [144] P. B. Denton and J. Gehrlein, *New oscillation and scattering constraints on the tau row matrix elements without assuming unitarity*, *JHEP* **06** (2022) 135, [[arXiv:2109.14575](#)].
- [145] P. B. Denton, *Tau neutrino identification in atmospheric neutrino oscillations without particle identification or unitarity*, *Phys. Rev. D* **104** (2021), no. 11 113003, [[arXiv:2109.14576](#)].
- [146] **IceCube** Collaboration, P. Eller et al., *Sensitivity of the IceCube Upgrade to Atmospheric Neutrino Oscillations*, *PoS ICRC2023* (2023) 1036, [[arXiv:2307.15295](#)].
- [147] **IceCube-Gen2** Collaboration, M. G. Aartsen et al., *IceCube-Gen2: the window to the extreme Universe*, *J. Phys. G* **48** (2021), no. 6 060501, [[arXiv:2008.04323](#)].
- [148] **KM3NeT** Collaboration, T. Eberl, S. Hallmann, and J. Hofestädt, *Tau neutrino appearance with KM3NeT/ORCA*, *PoS ICRC2017* (2018) 1025.
- [149] A. De Gouvêa, K. J. Kelly, G. V. Stenico, and P. Pasquini, *Physics with Beam Tau-Neutrino Appearance at DUNE*, *Phys. Rev. D* **100** (2019), no. 1 016004, [[arXiv:1904.07265](#)].
- [150] I. Esteban, M. C. Gonzalez-Garcia, M. Maltoni, T. Schwetz, and A. Zhou, *The fate of hints: updated global analysis of three-flavor neutrino oscillations*, *JHEP* **09** (2020) 178, [[arXiv:2007.14792](#)].
- [151] NuFIT 5.2 (2022), <http://www.nu-fit.org/>.
- [152] F. Capozzi, E. Di Valentino, E. Lisi, A. Marrone, A. Melchiorri, and A. Palazzo, *Unfinished fabric of the three neutrino paradigm*, *Phys. Rev. D* **104** (2021), no. 8 083031, [[arXiv:2107.00532](#)].
- [153] P. F. de Salas, D. V. Forero, S. Gariazzo, P. Martínez-Miravé, O. Mena, C. A. Ternes, M. Tórtola, and J. W. F. Valle, *2020 global reassessment of the neutrino oscillation picture*, *JHEP* **02** (2021) 071, [[arXiv:2006.11237](#)].
- [154] T. K. Gaisser and M. Honda, *Flux of atmospheric neutrinos*, *Ann. Rev. Nucl. Part. Sci.* **52** (2002) 153–199, [[hep-ph/0203272](#)].
- [155] A. Dziewonski and D. Anderson, *Preliminary Reference Earth Model*, *Phys. Earth Planet. Interiors* **25** (1981) 297–356.
- [156] A. de Gouvea, J. Jenkins, and B. Kayser, *Neutrino mass hierarchy, vacuum oscillations, and vanishing $U(e3)$* , *Phys. Rev.* **D71** (2005) 113009, [[hep-ph/0503079](#)].
- [157] H. Nunokawa, S. J. Parke, and R. Zukanovich Funchal, *Another possible way to determine the neutrino mass hierarchy*, *Phys. Rev.* **D72** (2005) 013009, [[hep-ph/0503283](#)].
- [158] R. Santonico and R. Cardarelli, *Development of resistive plate counters*, *Nuclear Instruments and Methods in Physics Research* **187** (1981), no. 2 377 – 380.
- [159] S. Bheesette, *Design and Characterisation Studies of Resistive Plate Chambers*. PhD thesis, Indian Inst. Tech., Mumbai, 2009.
- [160] M. Bhuyan et al., *Development of 2m x 2m size glass RPCs for INO*, *Nucl. Instrum. Meth. A* **661** (2012) S64–S67.
- [161] A. D. Bhatt, *Measurement of Atmospheric Muons at IICHEP in Madurai, for better estimation of Neutrino Fluxes at INO Site in Theni*. PhD thesis, HBNI, Mumbai, 2019.
- [162] D. Casper, *The Nuance neutrino physics simulation, and the future*, *Nucl. Phys. Proc. Suppl.* **112** (2002) 161, [[hep-ph/0208030](#)].

- [163] M. Sajjad Athar, M. Honda, T. Kajita, K. Kasahara, and S. Midorikawa, *Atmospheric neutrino flux at INO, South Pole and Pyhasalmi*, *Phys. Lett. B* **718** (2013) 1375–1380, [[arXiv:1210.5154](#)].
- [164] M. Honda, M. Sajjad Athar, T. Kajita, K. Kasahara, and S. Midorikawa, *Atmospheric neutrino flux calculation using the NRLMSISE-00 atmospheric model*, *Phys. Rev. D* **92** (2015), no. 2 023004, [[arXiv:1502.03916](#)].
- [165] N. Dash, *Feasibility studies for the detection of exotic particles using ICAL at INO*. PhD thesis, HBNI, Mumbai, 2015.
- [166] S. Pal, *Development of the INO-ICAL detector and its physics potential*. PhD thesis, HBNI, Mumbai, 2014.
- [167] M. Blennow, P. Coloma, P. Huber, and T. Schwetz, *Quantifying the sensitivity of oscillation experiments to the neutrino mass ordering*, *JHEP* **1403** (2014) 028, [[arXiv:1311.1822](#)].
- [168] M. C. Gonzalez-Garcia and M. Maltoni, *Atmospheric neutrino oscillations and new physics*, *Phys. Rev.* **D70** (2004) 033010, [[hep-ph/0404085](#)].
- [169] P. Huber, M. Lindner, and W. Winter, *Superbeams versus neutrino factories*, *Nucl. Phys.* **B645** (2002) 3–48, [[hep-ph/0204352](#)].
- [170] G. L. Fogli, E. Lisi, A. Marrone, D. Montanino, and A. Palazzo, *Getting the most from the statistical analysis of solar neutrino oscillations*, *Phys. Rev. D* **66** (2002) 053010, [[hep-ph/0206162](#)].
- [171] J. Kameda, *Detailed studies of neutrino oscillations with atmospheric neutrinos of wide energy range from 100 MeV to 1000 GeV in Super-Kamiokande*. PhD thesis, Tokyo U., 2002.
- [172] R. Gandhi, P. Ghoshal, S. Goswami, P. Mehta, S. U. Sankar, et al., *Mass Hierarchy Determination via future Atmospheric Neutrino Detectors*, *Phys.Rev.* **D76** (2007) 073012, [[arXiv:0707.1723](#)].
- [173] M. Blennow and T. Schwetz, *Identifying the Neutrino mass Ordering with INO and NOvA*, *JHEP* **1208** (2012) 058, [[arXiv:1203.3388](#)].
- [174] F. J. Escrivuela, D. V. Forero, O. G. Miranda, M. Tórtola, and J. W. F. Valle, *Probing CP violation with non-unitary mixing in long-baseline neutrino oscillation experiments: DUNE as a case study*, *New J. Phys.* **19** (2017), no. 9 093005, [[arXiv:1612.07377](#)].
- [175] P. Huber, M. Lindner, and W. Winter, *Simulation of long-baseline neutrino oscillation experiments with GLOBES (General Long Baseline Experiment Simulator)*, *Comput.Phys.Commun.* **167** (2005) 195, [[hep-ph/0407333](#)].
- [176] P. Huber, J. Kopp, M. Lindner, M. Rolinec, and W. Winter, *New features in the simulation of neutrino oscillation experiments with GLOBES 3.0: General Long Baseline Experiment Simulator*, *Comput.Phys.Commun.* **177** (2007) 432–438, [[hep-ph/0701187](#)].
- [177] M. Blennow and E. Fernandez-Martinez, *Neutrino oscillation parameter sampling with MonteCUBES*, *Comput. Phys. Commun.* **181** (2010) 227–231, [[arXiv:0903.3985](#)].
- [178] E. K. Akhmedov, R. Johansson, M. Lindner, T. Ohlsson, and T. Schwetz, *Series expansions for three flavor neutrino oscillation probabilities in matter*, *JHEP* **0404** (2004) 078, [[hep-ph/0402175](#)].

- [179] E. Fernandez-Martinez, J. Hernandez-Garcia, and J. Lopez-Pavon, *Global constraints on heavy neutrino mixing*, *JHEP* **08** (2016) 033, [[arXiv:1605.08774](#)].